

On the Variability of Concept Activation Vectors

Julia Wenkmann¹, Damien Garreau¹

¹Universität Würzburg, CAIDAS

julia.wenkmann@stud-mail.uni-wuerzburg.de, damien.garreau@uni-wuerzburg.de

Abstract

One of the most pressing challenges in artificial intelligence is to make models more transparent to their users. Recently, explainable artificial intelligence has come up with numerous method to tackle this challenge. A promising avenue is to use concept-based explanations, that is, high-level concepts instead of plain feature importance score. Among this class of methods, Concept Activation vectors (CAVs), Kim et al. (2018) stands out as one of the main protagonists. One interesting aspect of CAVs is that their computation requires sampling random examples in the train set. Therefore, the actual vectors obtained may vary from user to user depending on the randomness of this sampling. In this paper, we propose a fine-grained theoretical analysis of CAVs construction in order to quantify their variability. Our results, confirmed by experiments on several real-life datasets, point out towards an universal result: the variance of CAVs decreases as $1/N$, where N is the number of random examples. Based on this we give practical recommendations for a resource-efficient application of the method.

1 Introduction

Explainable Artificial Intelligence (XAI) has rapidly ascended to the forefront of machine learning research, as the field grapples with the challenge of making deep neural networks more transparent and trustworthy. Recently, explainable artificial intelligence has come up with numerous method to tackle this challenge. A promising avenue is to use concept-based explanations, that is, high-level concepts instead of plain feature importance score (Poeta et al. 2023). One method, that has risen to prominence in Concept-based Explainable Artificial Intelligence (C-XAI), is Testing with Concept Activation Vectors (TCAV), introduced by Kim et al. (2018). TCAV quantifies the influence of human-understandable concepts (*e.g.*, “stripes”) on a specific class (*e.g.*, “zebra”). The core of the method is the Concept Activation Vector (CAV). This vector defines the direction of a concept in a latent layer as the normal vector of a linear boundary between the embeddings of concept examples and a set of randomly selected reference data, so-called random samples. The resulting TCAV score measures the sensitivity of a prediction for this specific concept, as described in detail in Section 3.

A problem of XAI methods is their stability (also referred to as consistency). A method is considered stable if

it provides identical or at least similar explanations for the same model and input when applied repeatedly (Alvarez-Melis and Jaakkola 2018). Failure to meet this standard can lower the trust users place in the explanation, a known issue for many XAI techniques (Krishna et al. 2024). Due to its reliance on random sampling, TCAV’s results exhibit high variability from one run to another. Kim et al. (2018) acknowledged this issue and suggested running the method several times and reporting the average scores to mitigate the variability. However, this solution is not perfect, as the average itself is still subject to variance. This leads to a fundamental question regarding computational resources: how can the variance of the result be minimized within a limited sampling budget? In other words, is it more effective to conduct a single run with a large number of samples, or to average the outcomes of multiple runs, each using a smaller sample set?

To answer this question, we conduct the (first) theoretical analysis of the influence of the number of random samples on the variance of TCAV. Based on this, we derive practical recommendations for a resource-efficient application of the method.

Our contributions are as follows:

- **Asymptotic variability of CAVs.** In the infinitely imbalanced regime (fixed concept set, $N \rightarrow \infty$ random references) we prove asymptotic normality of the penalized logistic CAV estimator (Thm. 1). Under some reasonable assumptions, the covariance trace decays as $\mathcal{O}(1/N)$ (Cor. 4.2).
- **Sensitivity and TCAV.** The asymptotic normality transfers to sensitivity scores; Under the same assumptions, their variance scales as $\mathcal{O}(1/N)$, whereas TCAV may retain $\Theta(1)$ variance due to borderline evaluation points.
- **Multi-run averaging.** Averaging TCAV over s independent runs reduces variance as $\mathcal{O}(1/s)$ (Conj. 1); we discuss the effect of mild dependence.
- **Guidelines.** To stabilize TCAV, prefer several modest- N runs; to stabilize the CAV direction for downstream use, increase N per run.

We provide the code for all experiments in the supplementary material and will publicly release it after publication.

2 Related Work

As mentioned earlier, TCAV is a very influential method among concept-based explainability approaches and has been extended and modified several times (Poeta et al. 2023). For this reason, we focus on TCAV, since an analysis of its stability also cascades to its adaptations.

Influence of the (T)CAV method. Many subsequent works use both CAVs and TCAV scores to represent concepts in latent space and analyze class-concept relationships. For example, STCE (Ji, Wang, and Kato 2023) transfers the TCAV method to video data and thus allows a temporal view of concepts. Other methods, such as ACE (Ghorbani et al. 2019), ICE (Zhang et al. 2021) and COCoX (Akula, Wang, and Zhu 2020), adapt the calculation of the TCAV score, but in an unsupervised setting. Although TCAV provides mainly global class-concept relationships, CAVLI (Shukla, Bharati, and Turk 2023) and Visual-TCAV (Santis et al. 2024) adapted it to produce local explanations. Specifically, CAVLI combines TCAV with LIME for instance-level interpretations, and Visual-TCAV adds saliency maps to localize concepts in the input, leveraging an Integrated Gradients (Sundararajan, Taly, and Yan 2017) approach.

Subsequent work has also focused on improving the accuracy of CAVs and accommodating non-linearly separable concepts, which can not be fully captured by CAVs. Methods like *Concept Activation Regions* (CAR) (Crabbé and van der Schaar 2022) and *Concept Gradient* (CG) (Bai et al. 2024) generalize CAVs to capture more complex concept boundaries, representing concepts through kernel-based regions or non-linear functions. Soni et al. (2020) improve CAV robustness in two ways. First, *Adversarial* CAV introduces small adversarial perturbations to concept samples. This leads to more stable concept vectors. Second, *Orthogonal Adversarial* CAV applies a Gram–Schmidt-like orthogonalization to further separate concept and non-concept subspaces, thus improving CAV separability. Pattern-based CAVs, introduced by Pahde et al. (2024), address the issue of noise when learning CAVs. Instead of learning to separate positive and negative examples, they find a direction in activation space that best correlates with a concept’s intensity. This, together with sparsity constraints, yields concept representations that are more precise and robust against noise.

Finally, researchers such as Pahde et al. 2022, Dreyer et al. 2023, and Bareeva et al. 2024 have also used TCAV to improve model performance and mitigate bias. They use Concept Activation Vectors to identify and remove undesirable concepts that the model learned during training.

Prior Theoretical Analysis of XAI. An important part of evaluating XAI methods is examining their consistency, *i.e.*, the extent to which an explanation method provides deterministic explanations for the same inputs to be explained. Such an analysis has already been carried out for some established XAI methods, such as LIME (Ribeiro, Singh, and Guestrin 2016). Garreau and Mardaoui (2021) show that the randomness and instability observed in LIME explanations are a direct result of not using enough samples to fit the linear model. When the number of generated samples is very

large, the explanations converge to an explicit “limit explanation.” Visani et al. (2021) take a different approach by introducing two new indices to measure the instability and reliability of LIME. These indices give practitioners a tool to assess the trustworthiness of LIME’s outputs, which is demonstrated using a credit risk case study.

Although Concept Activation Vectors are widely used, their fundamental properties and limitations have been underexplored, with only few works systematically addressing this gap (Nicolson et al. 2025). Key issues affecting the reliability and interpretability of CAVs include layer inconsistency (Nicolson et al. 2025), concept entanglement (Chen, Bei, and Rudin 2020), dependence on the spatial location of the concept (Raman, Espinosa Zarlenga, and Jamnik 2024), and sensitivity to data variations (Ramaswamy et al. 2023, Soni et al. 2020).

In this paper, we extend the last point, the *sensitivity to data variations*. For this, we systematically analyze the variance of CAVs. In particular, we investigate how the number of random samples affects the stability of the calculated CAVs. To the best of our knowledge, there has been no throughout investigation of this topic to date.

3 Preliminaries and Notation

In this section, we describe the concept activation vectors and TCAV values utilised by Kim et al. (2018) and thereby introduce our notation.

3.1 Generating Concept Activation Vectors

We can understand how a model works by looking at the concepts it learns in its hidden layers. For instance, a network might identify “stripes” as an important concept when classifying an image as a “zebra”. To formalize this, we split our model $f: \mathcal{X} \rightarrow \mathbb{R}^K$ intended for the classification of K classes, into two parts $f := g_\ell \circ h_\ell$, at a specific layer ℓ . Here $h_\ell: \mathcal{X} \rightarrow \mathbb{R}^d$ is the model up to layer ℓ , and $g_\ell: \mathbb{R}^d \rightarrow \mathbb{R}^K$ is the remaining part of the network, which transforms the embedding vectors in the latent space \mathbb{R}^d into class logits. In other words, for a fixed class $k \in \{1, \dots, K\}$, the function $g_{\ell,k}: \mathbb{R}^d \rightarrow \mathbb{R}$ maps a latent embedding $v \in \mathbb{R}^d$ to the logit (or score) of class k . This is illustrated in Figure 1.

To compute the CAV in layer ℓ , we collect:

1. *Positive examples* of concept C , *i.e.*, a set of n inputs $\{x_i\}_{i=1}^n \subset \mathcal{X}$ that clearly exhibit the concept C . These examples can be sourced from annotated datasets, like the Broden dataset (Bau et al. 2017), or be custom-curated for the specific concept under study.
2. *Negative (random) examples*, *i.e.*, a set of N inputs $\{z_j\}_{j=1}^N \subset \mathcal{X}$ selected uniformly among the training set.

We then compute the latent embeddings of the concepts and the random examples. Since raw feature vectors do not trivially encode the presence or absence of a concept C , TCAV trains a linear classifier to discriminate between positive $\{h_\ell(x_i)\}_{i=1}^n$ and negative $\{h_\ell(z_j)\}_{j=1}^N$ embeddings. The normal vector to the decision boundary learned by the classifier, oriented towards the concept examples, is defined as the Concept Activation Vector v_C^ℓ of concept C . Note,

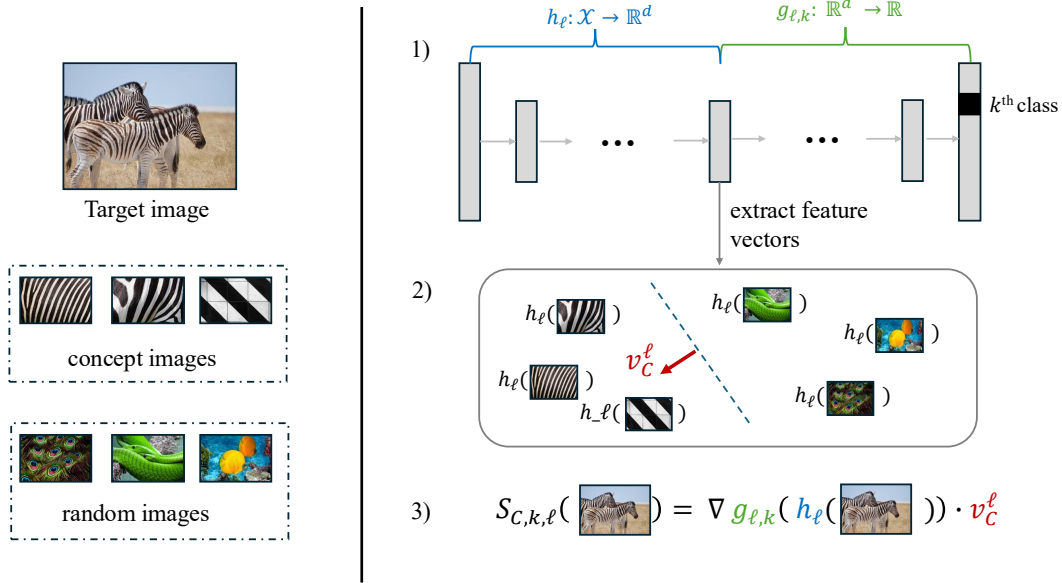


Figure 1: An overview of the first part of the TCAV operating procedure: 1) TCAV extracts the activation vectors at a specific layer ℓ . 2) The CAV v_C^ℓ , shown by the red arrow, is learned by training a binary linear classifier to differentiate between concept examples and random examples. 3) TCAV calculates the directional derivative $S_{C,k,\ell}(x)$ to measure how sensitive the model’s class prediction is to the Concept Activation Vector v_C^ℓ .

that the CAV depends on both the random sampling and the stochastic nature of the classifier training process. Several different classifiers can be employed:

- The original TCAV implementation defaults to a linear Support Vector Machine (SGDClassifier with hinge loss (Pedregosa et al. 2011)), as detailed in Appendix B.2.
- A simpler approach, Difference of Means, proposed by Martin (2019), is adopted in Visual-TCAV (Santis et al. 2024). It calculates the CAV as the difference between the mean embeddings of the concept and random samples. Santis et al. report that this estimator yields better CAV quality. This case is discussed in Appendix B.3.

Despite the differences in these models, all of those different classifiers exhibit the same asymptotic normality behaviour, as demonstrated experimentally in Appendix A. However, in this paper, we focus on LogisticRegression with binary cross-entropy loss. We choose this method because it presents a more amenable mathematical analysis and is another prominent classifier available in the official TCAV libraries (Kokhlikyan et al. 2020, Kim et al. 2025).

3.2 Calculating TCAV Scores

Once the CAV v_C^ℓ has been determined for the concept C in the layer ℓ , TCAV then evaluates the relevance of this concept for a class k by comparing the gradient of $g_{\ell,k}$ with the direction of v_C^ℓ using the dot product (\cdot) . Specifically, for an input $\mathbf{x} \in \mathcal{X}_k$, that is, an input \mathbf{x} of class k , TCAV defines

the *sensitivity score* of \mathbf{x} as

$$S_{C,k,\ell}(\mathbf{x}) := \nabla g_{\ell,k}(h_\ell(\mathbf{x})) \cdot v_C^\ell. \quad (1)$$

The score $S_{C,k,\ell}(\mathbf{x})$ measures a concept’s influence on the classification of \mathbf{x} . A positive score means the concept pulls the prediction toward class k , while a negative score pushes it away. To aggregate these local sensitivities, the TCAV score is defined as the proportion of samples \mathbf{x} from the class k whose sensitivity $S_{C,k,\ell}(\mathbf{x})$ is positive, that is,

$$\text{TCAV}_{C,k,\ell} := \frac{|\{\mathbf{x} \in \mathcal{X}_k \mid S_{C,k,\ell}(\mathbf{x}) > 0\}|}{|\mathcal{X}_k|}. \quad (2)$$

A score close to 1 means concept C shifts the classification toward class k , a low score (close to 0) indicates a strong negative effect, while a score near 0.5 implies no consistent effect. Finally, a two-tailed t -test (see, e.g., (Hogg, McKean, and Craig 2019), Chapter 4.5) is performed on the sensitivity values to ensure that the effect captured by the TCAV score is not due to random variation.

4 Theoretical analysis

We now present our main theoretical results regarding the variability of CAVs obtained by logistic regression when the number of random examples goes to infinity. This reflects the practice well: in applications, the number of annotated concepts is usually restricted (for instance, a typical concept class in the Broden dataset has on average 50 examples (Bau et al. 2017)), whereas the number of random examples is virtually unlimited (the ImageNet dataset has 10^6 images

(Deng et al. 2009)). Therefore, we analyse the stability of CAVs in this (infinitely) imbalanced setting.

Let us now define the formal setting for our analysis.

4.1 Theoretical setting

We consider two sets of feature vectors:

- **n fixed points**, $\{x_i\}_{i=1}^n$, which represent our “concept” samples and are assigned the class label $Y = 1$.
- **N random points**, $\{z_j\}_{j=1}^N$, which are drawn from the distribution F_0 of training samples and assigned the class label $Y = 0$.

For simplicity, we use $\{x_i\}_{i=1}^n$ and $\{z_j\}_{j=1}^N$ as shorthand for their respective latent representations, $\{h_\ell(x_i)\}$ and $\{h_\ell(z_j)\}$ in the definitions above as well as throughout the rest of this paper. We denote the *intercept* by $\alpha \in \mathbb{R}$ and the *coefficients* by $\beta \in \mathbb{R}^d$. Following Owen (2007), for any input $w \in \mathbb{R}^d$, we write the logistic regression model as

$$\mathbb{P}(Y = 1 | X = w) = \sigma(\alpha + \beta^\top w), \quad (3)$$

where $\sigma(u) := (1 + e^{-u})^{-1}$, with $u \in \mathbb{R}$. For any given N , we fit the logistic regression model Eq. (3) by maximizing the L^2 -penalized log-likelihood

$$\begin{aligned} \mathcal{L}_N^{(\lambda)}(\alpha, \beta) := & \sum_{i=1}^n \log \sigma(\alpha + \beta^\top x_i) \\ & + \sum_{j=1}^N \log(1 - \sigma(\alpha + \beta^\top z_j)) - \frac{\lambda}{2} \|\beta\|^2, \end{aligned} \quad (4)$$

where λ is the regularization parameter. We denote by (α_N, β_N) the unique maximizer of this function. The theoretical coefficient β_N corresponds exactly to our empirical CAV v_C^ℓ calculated with N random samples. Note, however, that our analysis does not consider any effects from the optimisation procedure.

4.2 Variability of Concept Activation Vectors

In this section, we prove asymptotic normality of CAVs in the special case of infinite imbalance. This specific logistic regression setting, where the number of samples in one class grows infinitely large while the other is held fixed, was previously analyzed by Owen (2007) and Goldman and Zhang (2022). Our result, similar to that of Owen (2007), is conditional upon the “Surrounded Mean” Assumption 1. This is a weak condition, postulating that infinite random samples surround the concept’s mean \bar{x} in the latent space, which generally holds in practice (see Appendix B.1).

Assumption 1 (Surrounded Mean). *The distribution F_0 on \mathbb{R}^d has the point \bar{x} “surrounded,” that is*

$$\int_{(z-\bar{x})^\top \omega > \varepsilon} dF_0(z) > \delta \quad (5)$$

holds for some $\varepsilon > 0$, some $\delta > 0$ and all $\omega \in \Omega$ where $\Omega = \{\omega \in \mathbb{R}^d | \omega^\top \omega = 1\}$ is the unit sphere in \mathbb{R}^d and \bar{x} is the mean of the concept embeddings $\{x_i\}_{i=1}^n$.

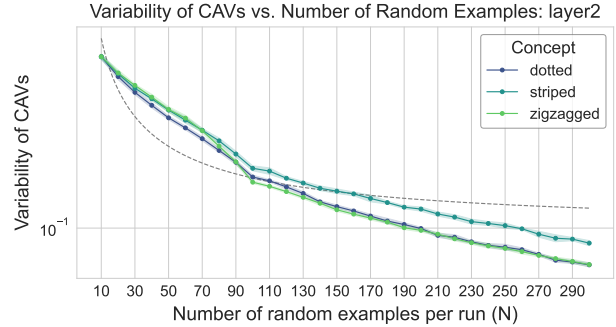


Figure 2: Mean variability of CAVs for ResNet at layer ‘layer2’ as a function of the number of random examples per run (N), shown for “striped”-, “zigzagged”-, and “dotted” concepts. Error bars indicate ± 1 standard deviation; the y -axis is log-scaled. Variance of CAVs is estimated by taking the sum of per-feature variances across ten independent runs. The dashed line shows a theoretical fit of the form $y = a/N + b$.

This mild geometric condition says that, in every direction, the random references populate a non-trivial cap around \bar{x} . Our second assumption is a technical one. We assume that the limit of the Hessian of Eq. (4) is exists and invertible, which is a standard condition in the analysis of maximum likelihood estimators.

Assumption 2 (Limit Hessian). *Assume that the matrix H_0 , defined as the limit in probability of the normalized Hessian of the loss function,*

$$H_0 := \lim_{N \rightarrow \infty} \left(-\frac{1}{N} \nabla_\beta^2 \mathcal{L}^{(\lambda)}(\alpha_N, \beta_N) \right)$$

exists and is invertible.

We can now state our main result:

Theorem 1 (Asymptotic variability of CAVs). *Assume that Assumptions 1 and 2 hold, that the limit $A_0 = \lim_{N \rightarrow \infty} N e^{\alpha_N}$ exists and that $\beta_N \xrightarrow{p} \beta_0$, where \xrightarrow{p} denotes convergence in probability as $N \rightarrow \infty$. Then β_N is asymptotically normal. Namely,*

$$\sqrt{N}(\beta_N - \beta_0) \xrightarrow{D} \mathcal{N}(0, \Sigma), \quad (6)$$

where \xrightarrow{D} denotes convergence in distribution. A precise expression of Σ is given in Appendix B.1 (Eq. (18)).

Informally, this means that for large values of N , $\sqrt{N}(\beta_N - \beta_0)$ behaves as a multivariate normal distribution $\mathcal{N}(0, \Sigma)$. This finding is consistent with standard statistical theory. The CAV β_N behaves like a logistic regression estimator (Goldman and Zhang 2022), whose variance is known to scale inversely with the sample size.

Let us now return to our central topic: the variability of the CAVs. A direct consequence of Theorem 1 is that the CAVs become more stable with increasing number N of random samples used. Coming back to variability, we choose the trace of the covariance matrix of the CAVs, i.e., the sum

of the per-feature variance, as a variability measure. This measure will equal zero, *if and only if* the CAVs had no variability at all.

Definition 1 (Variance of CAVs). *We define the variance of β_N as*

$$\begin{aligned}\text{Var}(\beta_N) &:= \sum_j \text{Cov}(\beta_N)_{jj} \\ &= \sum_j \mathbb{E} \left[(\beta_N - \mathbb{E}[\beta_N]) (\beta_N - \mathbb{E}[\beta_N])^\top \right]_{jj}.\end{aligned}$$

Using this definition, we are now able to examine the variability of CAVs.

Asymptotic Behavior of the Covariance Trace Theorem 1 gives $\sqrt{N}(\hat{\beta}_N - \beta_0) \Rightarrow \mathcal{N}(0, \Sigma)$. Assuming, that the sequence $\{\sqrt{N}(\hat{\beta}_N - \beta_0)\}_{N \geq 1}$ is uniformly integrable, this entails $\text{Var}(\hat{\beta}_N)(\hat{\beta}_N) = \mathcal{O}(\frac{1}{N})$. See Appendix B.1, Corollary 4.2 for a precise statement and proof. Essentially, this means that as the random dataset size (N) grows, the variability in the direction of the Concept Activation Vector (β_N) shrinks at a rate proportional to $1/N$. For instance, multiplying the number of random examples N by ten reduces the variance of the estimator by a factor of ten. This is in accordance with our experimental results presented in Figure 2. Additional experimental findings for different datasets and models are presented in Section 5.

Sketch of the proof of Theorem 1. The proof uses and adapts methods from (Owen 2007) and (Goldman and Zhang 2022). The main difference with their work is that we take the L^2 penalization of the objective (4) into account, thus extending their results. This leads to a different, but still asymptotically normal convergence behaviour in $\mathcal{O}(N^{1/N})$. We proceed as follows: First, we perform a *Taylor-expansion* on the gradient of our loss function (4) at the optimum, where $\nabla_{\beta} \mathcal{L}^{(\lambda)}(\beta_N) = 0$, around the true parameter β_0 . This allows us to express $\sqrt{N}(\beta_N - \beta_0)$ as the product of the inverse Hessian and the scaled score. Then, the normalized Hessian converges to a constant by the Law of Large Numbers. Vitally, the scaled score converges to a zero-mean normal distribution via the Central Limit Theorem, as the term from the L^2 -penalty is perfectly cancelled by the score's expectation. Slutsky's Theorem (Slutsky 1937) then combines these results to establish the asymptotic normality of β_N . The full proof is provided in Appendix B.1. \square

4.3 Variance of Sensitivity Scores

We now analyze whether the asymptotic normality of CAVs transfers to the sensitivity scores. We restate them as

$$S(\mathbf{x}, \beta_N) := \nabla g_{\ell, k}(h_{\ell}(\mathbf{x})) \cdot \beta_N. \quad (7)$$

The following corollary shows that we can transfer the asymptotic convergence of the CAVs. The variance of the sensitivity score decreases at the rate $\mathcal{O}(1/N)$, like the variance of β_N , as demonstrated in Figure 3.

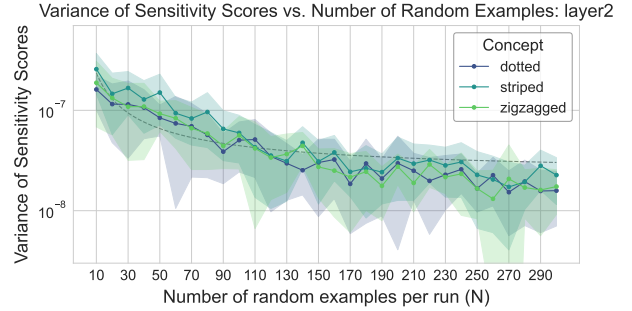


Figure 3: Mean variance of sensitivity scores vs. number N of random samples used for the class “zebra” in the Imagenet classification setting for one input. The y -value shows the geometric mean variance of these sensitivity scores ± 1 standard deviation, averaged over all $r = 10$ runs for a fixed positive input of a zebra. Log scale cut at $\geq 3 \times 10^{-9}$ so near-zero bands don't dominate.

Corollary 1 (Asymptotic variance of the Sensitivity Scores). *Under the conditions specified in Theorem 1, the sensitivity score $S(\mathbf{x}, \beta_N)$ satisfies*

$$Z_N := \sqrt{N} (S(\mathbf{x}, \beta_N) - S(\mathbf{x}, \beta_0)) \xrightarrow{D} \mathcal{N}(0, V(\mathbf{x})), \quad (8)$$

where the asymptotic variance $V(\mathbf{x})$ is given by

$$V(\mathbf{x}) := \nabla g_{\ell, k}(h_{\ell}(\mathbf{x}))^\top \cdot \Sigma \cdot \nabla g_{\ell, k}(h_{\ell}(\mathbf{x})). \quad (9)$$

This corollary is a direct consequence of Theorem 1 and the properties of multivariate normal distributions. Since the sensitivity score $S(\mathbf{x}, \beta_N)$ is a linear transformation (specifically, a dot product) of the random vector β_N , the asymptotic normality of $\sqrt{N}(\beta_N - \beta_0)$ transfers directly to the scaled sensitivity scores. The variance of the sensitivity score therefore diminishes at a rate of $\mathcal{O}(1/N)$, confirming that a larger sample size also yields more stable and trustworthy sensitivity scores, besides improved CAVs.

4.4 Variance of TCAV Scores

Extending our variance analysis to the TCAV scores in Equation (2), we make a surprising observation. In practice, the variance does not always decrease with more random samples, as one might assume. This means that, experimentally, the variance of the TCAV scores is approximately independent of the number N of random embedding vectors used (see Figure 4).

Our intuition for this quite surprising fact is, that across the embeddings of samples from a specific class, over which we calculate the TCAV score, a subset of them may lie **on** or **near** the decision boundary. This makes their classification highly sensitive to small changes in the model. Those samples, which we call “borderline points”, therefore still contribute to the variance of the TCAV score. This holds even when the variance of the CAVs vanishes asymptotically. For any other “non-borderline” point, the classification is asymptotically stable, and its contribution to the variance is negligible. The covariance between any two borderline points, on the other side, is a constant value, $\mathcal{O}(1)$, that

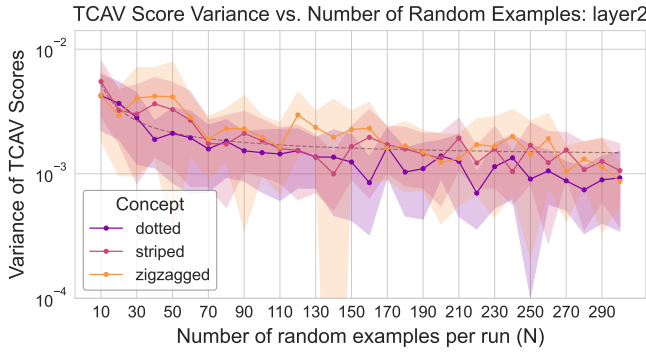


Figure 4: Mean variance of TCAV scores at layer ‘layer2’ vs. the number of random examples per concept set N for “striped”-, “zigzagged”-, and “dotted” concepts on the Imagenet dataset; error bars denote ± 1 standard deviation. Y -axis clipped at $\geq 10^{-4}$ to reduce distortion from near-zero standard deviations.

does not decrease as the CAV estimate improves. Therefore, the total variance is dominated by the sum over the pairs of “borderline points” and $\text{Var}(\text{TCAV}) = \mathcal{O}(1)$. More examples of this behavior are provided in Appendix A. Based on our empirical and theoretical observations we can now give concrete recommendations for action.

4.5 Recommendations for practice

Kim et al. (2018) already incorporated into their official implementation the method of running the TCAV algorithm multiple times with s different random sets and then calculating the mean value of the obtained TCAV scores. Precisely, the multi-run approach partitions a set of R random samples into s disjoint subsets, each of size $N = R/s$. For each subset $\in [1, \dots, s]$, a separate logistic regression is trained to find a CAV $\beta_N^{(j)}$. This yields s individual TCAV scores

$$T_j := \text{TCAV}(\beta_N^{(j)}) = \frac{|\{x \in \mathcal{X}_k \mid S(x, \beta_N^{(j)}) > 0\}|}{|\mathcal{X}_k|}.$$

The final **multi-run TCAV score**, T_{multi} , is the average of these individual scores $T_{\text{multi}} := \frac{1}{s} \sum_{j=1}^s T_j$. Based on our observations, averaging TCAV scores over multiple runs is indeed the most favourable method. Our analysis shows that as s increases, the variance decreases as $\mathcal{O}(1/s)$ (see Figure 5). This empirical finding aligns well with our theoretical expectations, as described below in Conjecture 1.

Conjecture 1. *Assuming $\text{Var}(\text{TCAV}) = \mathcal{O}(1)$, the variance of the multi-run score T_{multi} scales inversely with the number of subsets s :*

$$\text{Var}(T_{\text{multi}}) = \mathcal{O}\left(\frac{1}{s}\right).$$

Intuition. computations (Hogg, McKean, and Craig 2019). The CAVs $\beta_N^{(j)}$ are trained on disjoint (and thus independent) sets of random data, so the resulting TCAV

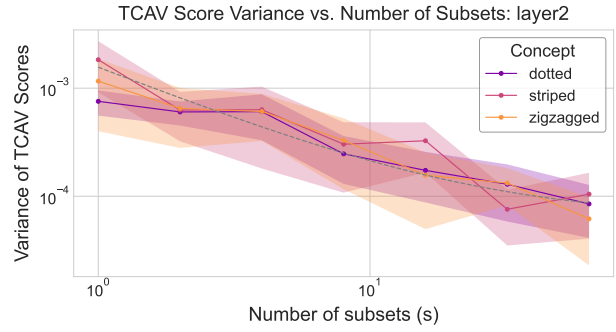


Figure 5: Variance of multi-run TCAV scores. We use a fixed number $R = 2000$ of random tabular samples and divide them over a varying number of subsets s , with each subset containing $N = R/s$ samples. To get the variance of the mean over all s TCAV scores, we repeat this $r = 10$ times and calculate the variance for each s over the r runs. The plot shows that the variance of the mean TCAV score decreases as s increases, confirming our theoretical analysis. Finally, we repeat this experiment $e = 10$ times and report the mean variance over those e runs ± 1 geometric standard deviation.

scores T_j can be treated as independent random variables. For s independent estimates T_1, \dots, T_s , each with variance $\sigma^2 = \text{Var}(T_j)$, the variance of their sample mean is $\text{Var}(T_{\text{multi}}) = \frac{\sigma^2}{s}$. Assuming $\sigma^2 = \mathcal{O}(1)$, the conjecture follows directly.

This provides practitioners with a tool for achieving the best possible stability with a fixed number of random samples. However, this comes at the expense of computing time. For example, the overhead in the Captum implementation (Kokhlikyan et al. 2020) means that doubling the number of subsets s halves the variance, but also increases the computing time linearly (in this case by a factor of ≈ 1.5).

5 Experiments

We test our theoretical findings across three data modalities: **images**, **tabular**, and **text** data. For all three data types we use appropriate datasets where concept samples are available. To assess the empirical variance of CAVs, we design the following experiment, which was repeated r times for statistical significance. For a given run, we vary the number of random examples, N . At each value of N , we compute s separate CAVs. Each of these CAVs was trained on a set of N examples, which were sampled with replacement from a large pool of 1,000 (for images) to 50,000 (for text) samples. We then calculate the trace of the covariance matrix of the resulting 10 CAVs. Finally, we report the mean and standard deviation of the traces collected across all $r = 10$ runs.

5.1 Image Classification

Following the original TCAV setup of Kim et al. (2018), we use the **ImageNet dataset** (Deng et al. 2009) and Broden (Bau et al. 2017) concept definitions. As a model

we use the pre-trained ResNet model (He et al. 2016). We evaluate our results in the layers '`inception4c`' and '`inception4e`'. For each concept ("striped", "zigzagged" and "dotted"), we calculate CAVs for an increasing number N (10 to 200) of random samples. We repeat the whole process $r = 5$ times with $m = 10$ random sets per run. The results can be found in Appendix A.1.

5.2 Tabular Data

To demonstrate applicability beyond vision, we adapt the framework to income prediction on the **UCI Adult dataset** (Becker and Kohavi 1996). Here we analyze how the demographic concepts of "male" and "female" are encoded within the model's hidden layers. The model is a custom two-layer feed-forward network trained to classify whether an individual's income exceeds 50,000\$ per year. We analyze CAVs for two target hidden layers, '`layer1`' and '`layer2`'. To test the stability of these conceptual representations, CAVs are generated multiple times under varying conditions. For tabular data, we vary the number of example samples from 10 to 300. For each value of N , the process is repeated for $r = 10$ independent runs with $m = 10$ random sets per run to ensure statistical significance. We present the results in Appendix A.2.

5.3 Text Classification

Finally, we apply CAVs in the NLP setting using the **IMDB sentiment dataset** (Maas et al. 2011). For this, we load a pre-trained text classifier (Kokhlikyan et al. 2020) and extract token embeddings. Concepts are defined by hand-picked sets of "positive", "negative", and "neutral" adjectives. We again use the same hyperparameters as for tabular data and report the variability of our CAVs and subsequent methods over $r = 10$ independent runs with N from 10 to 300. We provide the results for the layers '`conv1`' and '`conv2`' in Appendix A.3.

5.4 Results

In all three domains, the empirical variance of the CAV estimator decays approximately as $1/N$, in agreement with our theoretical $\mathcal{O}(1/N)$ prediction under uniform integrability. Furthermore, in all three domains, the variance of the TCAV scores becomes clearly stable, either immediately or after a short initial decrease. The TCAV method therefore does not directly use the information provided by increasingly accurate CAVs. We provide the Python code for all experiments in the supplementary material. The corresponding plots for the **hinge** and **binary cross-entropy** loss functions can be found in Appendix A. We decided not to conduct a separate experimental evaluation for **Difference of Means** method, as equivalent results can be expected due to the clear theoretical derivation (see Appendix B.2) and the demonstrated independence from the optimizer. This remains a task for future work.

6 Conclusion

In this paper, we analyze the stability of the TCAV method. To this end, we introduce a mathematical framework to the-

oretically analyze variability in the limit of infinitely imbalanced logistic regression, which applies beyond the scope of this work. Building on this analysis and extensive experiments, we provide practical recommendations on how many random samples to use and how to allocate them for optimal stability in TCAV. We further present a thorough exploration of the compute-consistency trade-off, quantifying how a fixed budget is best split between (i) more independent runs with fewer random samples per run and (ii) fewer runs with larger per-run sample sizes. *Crucially, this trade-off is method- and implementation-dependent*: it differs for TCAV scores versus CAVs and varies with the logistic-regression solver, regularization, feature normalization, and stopping criteria. We demonstrate that, for stable TCAV scores, a modest number of random samples distributed across multiple independent runs is sufficient and compute-efficient. By contrast, applications that require stable CAVs, such as bias mitigation or feature steering, benefit more from larger per-run sample sizes than from additional runs. We emphasize again that there is no single best setting: the optimal compute allocation should be re-evaluated for the specific method and implementation at hand.

Building on our findings, we identify two primary directions for future work. First, the nature of the trade-off between compute time and stability is highly implementation-dependent. We therefore propose investigating this trade-off in more detail to provide implementation-specific advice. Second, since our analysis assumed perfect optimization, an important goal for future work is to investigate the role of the optimizer. In particular, it would be interesting to examine the interaction between its convergence properties and the statistical stability of the resulting explanation.

References

Akula, A.; Wang, S.; and Zhu, S.-C. 2020. CoCoX: Generating Conceptual and Counterfactual Explanations via Fault-Lines. *Proceedings of the AAAI Conference on Artificial Intelligence*, 34(03): 2594–2601.

Alvarez-Melis, D.; and Jaakkola, T. S. 2018. On the Robustness of Interpretability Methods. Cite arxiv:1806.08049Comment: presented at 2018 ICML Workshop on Human Interpretability in Machine Learning (WHI 2018), Stockholm, Sweden.

Bai, A.; Yeh, C.-K.; Ravikumar, P.; Lin, N. Y. C.; and Hsieh, C.-J. 2024. Concept Gradient: Concept-based Interpretation Without Linear Assumption. In *International Conference on Learning Representations (ICLR)*.

Bareeva, D.; Dreyer, M.; Pahde, F.; Samek, W.; and Lapuschkin, S. 2024. Reactive Model Correction: Mitigating Harm to Task-Relevant Features via Conditional Bias Suppression.

Bau, D.; Zhou, B.; Khosla, A.; Oliva, A.; and Torralba, A. 2017. Network Dissection: Quantifying Interpretability of Deep Visual Representations. In *Proceedings of the IEEE Conference on Computer Vision and Pattern Recognition*, 3319–3327. IEEE Computer Society.

Becker, B.; and Kohavi, R. 1996. Adult. UCI Machine Learning Repository.

Chen, Z.; Bei, Y.; and Rudin, C. 2020. Concept Whitening for Interpretable Image Recognition. *Nature Machine Intelligence*, 2(12): 772–782.

Crabbé, J.; and van der Schaar, M. 2022. Concept Activation Regions: A Generalized Framework For Concept-Based Explanations. In *Proceedings of the 36th International Conference on Neural Information Processing Systems*, NIPS '22. Red Hook, NY, USA: Curran Associates Inc.

Deng, J.; Dong, W.; Socher, R.; Li, L.-J.; Li, K.; and Fei-Fei, L. 2009. ImageNet: A large-scale hierarchical image database. In *2009 IEEE Conference on Computer Vision and Pattern Recognition*, 248–255.

Dosovitskiy, A.; Beyer, L.; Kolesnikov, A.; Weissenborn, D.; Zhai, X.; Unterthiner, T.; Dehghani, M.; Minderer, M.; Heigold, G.; Gelly, S.; Uszkoreit, J.; and Houlsby, N. 2021. An Image is Worth 16x16 Words: Transformers for Image Recognition at Scale. In *International Conference on Learning Representations (ICLR)*.

Dreyer, M.; Pahde, F.; Anders, C. J.; Samek, W.; and Lapuschkin, S. 2023. From Hope to Safety: Unlearning Biases of Deep Models via Gradient Penalization in Latent Space.

Garreau, D.; and Mardaoui, D. 2021. What does LIME really see in images? In Meila, M.; and Zhang, T., eds., *Proceedings of the 38th International Conference on Machine Learning*, volume 139 of *Proceedings of Machine Learning Research*, 3620–3629. PMLR.

Ghorbani, A.; Wexler, J.; Zou, J. Y.; and Kim, B. 2019. Towards Automatic Concept-based Explanations. In *Advances in Neural Information Processing Systems*, volume 32. Curran Associates, Inc.

Goldman, D.; and Zhang, B. 2022. Asymptotic Inference for Infinitely Imbalanced Logistic Regression.

He, K.; Zhang, X.; Ren, S.; and Sun, J. 2016. Deep Residual Learning for Image Recognition. In *Proceedings of the IEEE Conference on Computer Vision and Pattern Recognition (CVPR)*, 770–778.

Hogg, R. V.; McKean, J. W.; and Craig, A. T. 2019. *Introduction to mathematical statistics*. Boston: Pearson, eighth edition edition. ISBN 978-0-13-468699-8.

Howard, A.; Sandler, M.; Chu, G.; Chen, L.-C.; Chen, B.; Tan, M.; Wang, W.; Zhu, Y.; Pang, R.; Vasudevan, V.; Le, Q.; and Adam, H. 2019. Searching for MobileNetV3. In *Proceedings of the IEEE/CVF International Conference on Computer Vision (ICCV)*.

Ji, Y.; Wang, Y.; and Kato, J. 2023. Spatial-Temporal Concept Based Explanation of 3D ConvNets. In *Proceedings of the IEEE/CVF Conference on Computer Vision and Pattern Recognition*, 15444–15453.

Kim, B.; Wattenberg, M.; Gilmer, J.; Cai, C.; Wexler, J.; Viegas, F.; and Sayres, R. 2018. Interpretability Beyond Feature Attribution: Quantitative Testing with Concept Activation Vectors (TCAV).

Kim, B.; Wattenberg, M.; Gilmer, J.; Cai, C.; Wexler, J.; Viegas, F.; and Sayres, R. 2025. Code for the TCAV ML interpretability project. Accessed on 2025-07-29.

Kokhlikyan, N.; Miglani, V.; Martin, M.; Wang, E.; Alsallakh, B.; Reynolds, J.; Melnikov, A.; Kliushkina, N.; Araya, C.; Yan, S.; and Reblitz-Richardson, O. 2020. Captum: A unified and generic model interpretability library for PyTorch.

Krishna, S.; Han, T.; Gu, A.; Wu, S.; Jabbari, S.; and Lakkaraju, H. 2024. The Disagreement Problem in Explainable Machine Learning: A Practitioner’s Perspective. *Transactions on Machine Learning Research*.

Maas, A. L.; Daly, R. E.; Pham, P. T.; Huang, D.; Ng, A. Y.; and Potts, C. 2011. Learning Word Vectors for Sentiment Analysis. In Lin, D.; Matsumoto, Y.; and Mihalcea, R., eds., *Proceedings of the 49th Annual Meeting of the Association for Computational Linguistics: Human Language Technologies*, 142–150. Portland, Oregon, USA: Association for Computational Linguistics.

Martin, T. 2019. *Interpretable Machine Learning*. M.phil. dissertation, University of Cambridge. Dept. of Engineering.

Nicolson, A.; Schut, L.; Noble, A.; and Gal, Y. 2025. Explaining Explainability: Recommendations for Effective Use of Concept Activation Vectors. *Transactions on Machine Learning Research*.

Owen, A. B. 2007. Infinitely Imbalanced Logistic Regression. *Journal of Machine Learning Research*, 8(4).

Pahde, F.; Dreyer, M.; Weber, L.; Weckbecker, M.; Anders, C. J.; Wiegand, T.; Samek, W.; and Lapuschkin, S. 2024. Navigating Neural Space: Revisiting Concept Activation Vectors to Overcome Directional Divergence.

Pahde, F.; Weber, L.; Anders, C.; Samek, W.; and Lapuschkin, S. 2022. *PatClArC: Using Pattern Concept Activation Vectors for Noise-Robust Model Debugging*.

Pedregosa, F.; Varoquaux, G.; Gramfort, A.; Michel, V.; Thirion, B.; Grisel, O.; Blondel, M.; Prettenhofer, P.; Weiss, R.; Dubourg, V.; Vanderplas, J.; Passos, A.; Cournapeau, D.; Brucher, M.; Perrot, M.; and Duchesnay, E. 2011. Scikit-learn: Machine Learning in Python. *Journal of Machine Learning Research*, 12(85): 2825–2830.

Poeta, E.; Ciravegna, G.; Pastor, E.; Cerquitelli, T.; and Baralis, E. 2023. Concept-based Explainable Artificial Intelligence: A Survey.

Raman, N. J.; Espinosa Zarlenga, M.; and Jamnik, M. 2024. Understanding Inter-Concept Relationships in Concept-Based Models. In Salakhutdinov, R.; Kolter, Z.; Heller, K.; Weller, A.; Oliver, N.; Scarlett, J.; and Berkenkamp, F., eds., *Proceedings of the 41st International Conference on Machine Learning*, volume 235 of *Proceedings of Machine Learning Research*, 42009–42025. PMLR.

Ramaswamy, V. V.; Kim, S. S. Y.; Fong, R.; and Russakovsky, O. 2023. Overlooked factors in concept-based explanations: Dataset choice, concept learnability, and human capability.

Ribeiro, M. T.; Singh, S.; and Guestrin, C. 2016. “Why Should I Trust You?”: Explaining the Predictions of Any Classifier. In *Proceedings of the 22nd ACM SIGKDD International Conference on Knowledge Discovery and Data Mining*, 1135–1144. San Francisco California USA: ACM.

Santis, A. D.; Campi, R.; Bianchi, M.; and Brambilla, M. 2024. Visual-TCAV: Concept-based Attribution and Saliency Maps for Post-hoc Explainability in Image Classification.

Shukla, P.; Bharati, S.; and Turk, M. 2023. CAVLI - Using image associations to produce local concept-based explanations. In *Proceedings of the IEEE/CVF Conference on Computer Vision and Pattern Recognition*, 3750–3755.

Slutzky, E. 1937. The Summation of Random Causes as the Source of Cyclic Processes. *Econometrica*, 5(2): 105–146.

Soni, R.; Shah, N.; Seng, C. T.; and Moore, J. D. 2020. Adversarial TCAV - Robust and Effective Interpretation of Intermediate Layers in Neural Networks. *CoRR*, abs/2002.03549.

Sundararajan, M.; Taly, A.; and Yan, Q. 2017. Axiomatic Attribution for Deep Networks. In *Proceedings of the 34th International Conference on Machine Learning*, 3319–3328.

Szegedy, C.; Liu, W.; Jia, Y.; Sermanet, P.; Reed, S.; Anguelov, D.; Erhan, D.; Vanhoucke, V.; and Rabinovich, A. 2014. Going Deeper with Convolutions.

Tan, M.; and Le, Q. V. 2019. EfficientNet: Rethinking Model Scaling for Convolutional Neural Networks. In *International Conference on Machine Learning (ICML)*, 6105–6114.

Vaart, A. W. v. d. 2007. *Asymptotic statistics*. Cambridge series in Statistical and Probabilistic Mathematics. Cambridge Univ. Press, 8. printing edition.

Visani, G.; Bagli, E.; Chesani, F.; Poluzzi, A.; and Capuzzo, D. 2021. Statistical stability indices for LIME: Obtaining reliable explanations for machine learning models. *Journal of the Operational Research Society*, 73: 1–11.

Zhang, R.; Madumal, P.; Miller, T.; Ehinger, K. A.; and Rubinstein, B. I. P. 2021. Invertible Concept-based Explanations for CNN Models with Non-negative Concept Activation Vectors. *Proceedings of the AAAI Conference on Artificial Intelligence*, 35(13): 11682–11690.

Appendix

Contents of the Appendix

Appendix	10
A Appendix A: Additional Results	10
A.1 TCAV for Images	10
A.2 TCAV for Tabular	12
A.3 TCAV for Text	15
B Appendix B: Proofs of the Main Results	18
B.1 Asymptotic Normality with Binary Cross-Entropy Loss	18
B.2 Asymptotic Normality with Hinge Loss	24
B.3 Asymptotic Normality of Difference of Means	25

A Appendix A: Additional Results

In the following we present additional experimental results regarding the variability of (T)CAVs varying the underlying linear classifier:

- First, we report additional results using the `LogisticRegression` classifier, which is optimized with a binary cross-entropy loss.
- Second, we report the same metrics `SGDLinearModel`, which is trained with a hinge loss.

For both sections, we show the variance of Concept Activation Vectors across two network layers. Moreover, sensitivity and TCAV scores are presented for a single representative layer, which we believe is sufficient to give a clear picture.

Note. All experiments were conducted on a MacBook Pro running macOS Sonoma 14.6. The system was equipped with an Apple M3 Max chip (14-core CPU) and 36 GB of unified memory.

A.1 TCAV for Images

Finally, we evaluate TCAV on images. We report results for ResNet50 (He et al. 2016), but the method is readily applicable to a wide range of architectures; we have also implemented it for GoogLeNet (Szegedy et al. 2014), EfficientNet (Tan and Le 2019), MobileNetV3 (Howard et al. 2019), and ViT-B/16 (Dosovitskiy et al. 2021). Across models, the empirical behavior aligns with our propositions and theorems, though to varying degrees. Some settings converge more slowly, which is expected given the asymptotic nature of our results.

Empirical Findings with Binary Cross-Entropy Loss Finally, we present the results for image data using the logistic regression classifier with binary cross-entropy loss. When analysing the variance with logistic regression classifiers, we observe a somewhat unexpected behaviour: initially, the variance increases until it asymptotically decreases after about 200 images. This is not a contradiction to our theoretical statements, as the latter only applies asymptotically. However, the exact reasons for this behaviour are worth investigating.

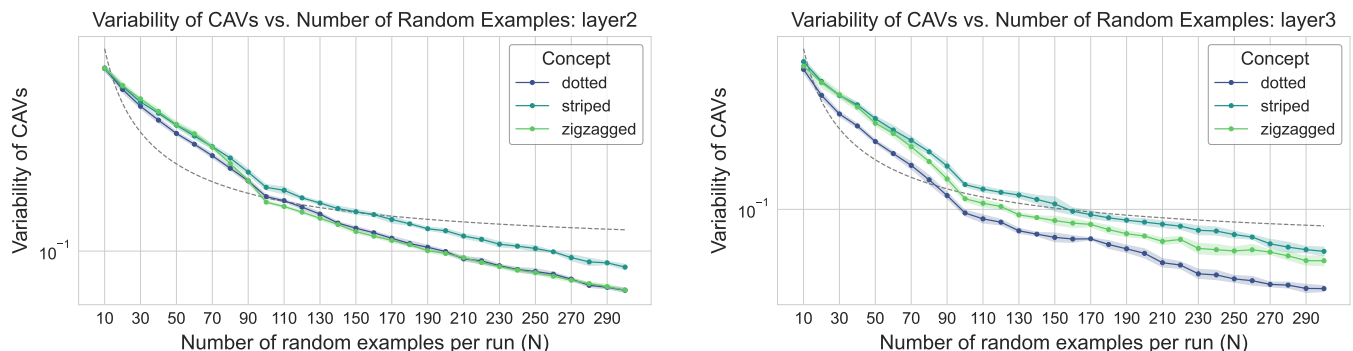


Figure 6: Mean variability of CAVs for “striped”, “zigzagged”, and “dotted” as a function of random examples (N) for ‘layer2’ and ‘layer3’ of the **Resnet50 model**. The classifiers were trained using **binary cross-entropy loss**. Error bars indicate ± 1 SD; the y -axis is log-scaled. We fitted a curve of the form $f(N) = a/N + b$ to it. For layer2 the parameters were $a = 7.71, b = 0.0999$, for layer3 they were $a = 5.58, b = 0.0643$.

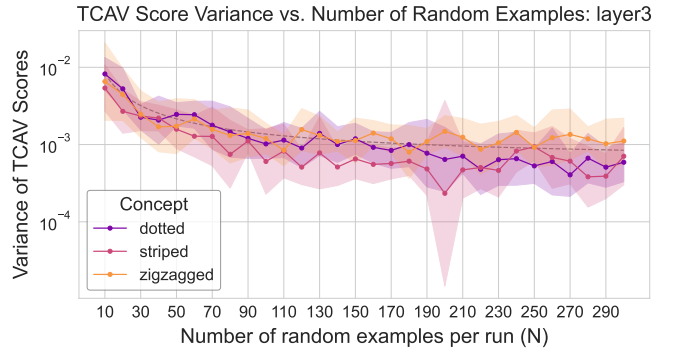
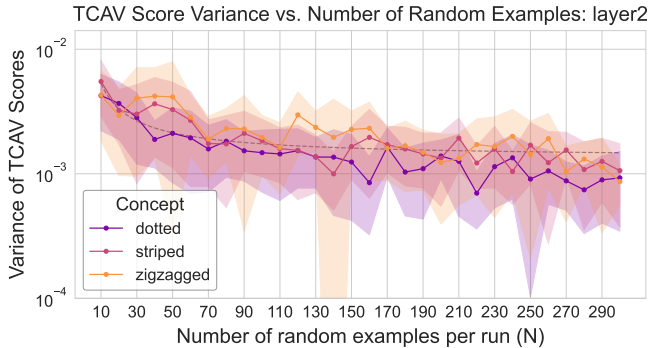


Figure 7: Variance of TCAV scores at ‘layer2’ and ‘layer3’ of the **Resnet50 model** vs. the number of examples per concept set (N) for the visual concepts “striped”, “zigzagged”, and “dotted”. Error bars denote ± 1 standard deviation. We fitted a curve of the form $f(N) = a/N + b$ to it. For layer2 the parameters were $a = 0.0396, b = 0.00134$, for layer3 they were $a = 0.0784, b = 5.83 \times 10^{-4}$. For layer2 the y -axis was clipped at $\geq 10^{-4}$.

Empirical Findings with Hinge Loss

Next, we show the corresponding results with hinge loss.

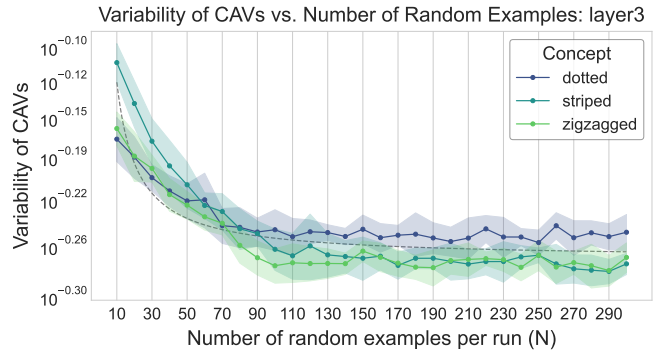
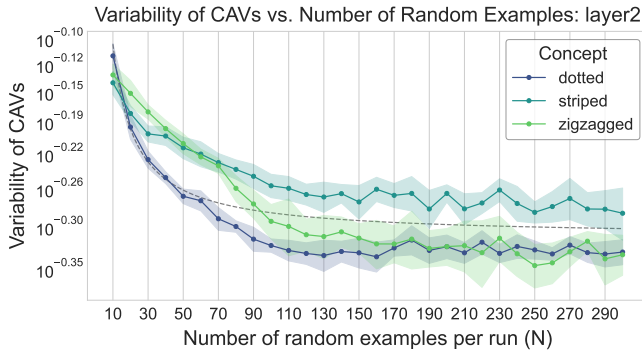


Figure 8: Mean variability of CAVs for the visual concepts “striped”, “zigzagged”, and “dotted” as a function of the number of random examples per run (N). Results are shown for two different layers of the **Resnet50 model** (‘layer2’ on the left, ‘layer3’ on the right). Error bars indicate ± 1 SD; the y -axis is log-scaled. Variance is estimated by the sum of per-feature variances across five independent runs. We fitted a curve of the form $f(N) = a/N + b$ to it. For layer2 the parameters were $a = 3.01, b = 0.488$, for layer3 they were $a = 2.12, b = 0.538$.

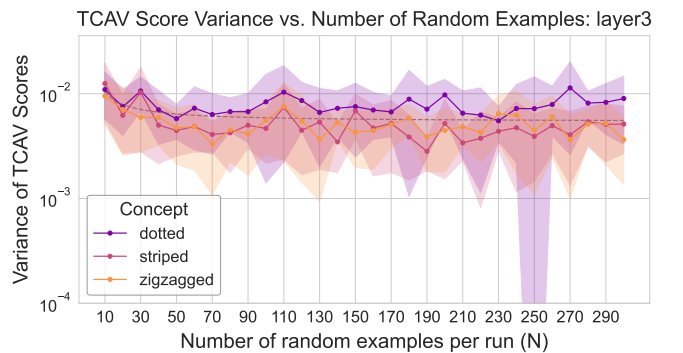
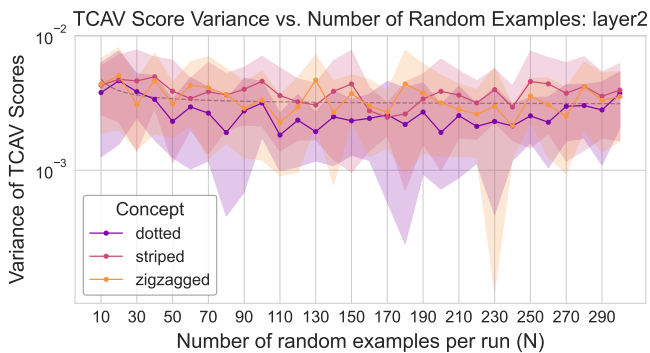


Figure 9: Variance of TCAV scores at ‘layer2’ and ‘layer3’ of the **ResNet50 model** vs. the number of examples per concept set (N) for the visual concepts “striped”, “zigzagged”, and “dotted”. The underlying CAVs were trained using **hinge loss**. Error bars denote ± 1 standard deviation. We fitted a curve of the form $f(N) = a/N + b$ to it. For layer2 the parameters were $a = 0.0168, b = 0.00307$, for layer3 they were $a = 0.0507, b = 0.00539$. For layer3 the scale is trimmed at $\geq 10^{-4}$ to prevent small-variance tails collapsing the plot. y -axis clipped at $\geq 10^{-6}$ for ‘layer2’ and $\geq 10^{-4}$ for layer3 to reduce distortion from near-zero standard deviations.

Empirical Findings with Difference of Means Again, we found that CAVs computed via the *Difference of Means*-method most closely follow a variance decline of $\mathcal{O}(1/N)$, compared to the other two methods.

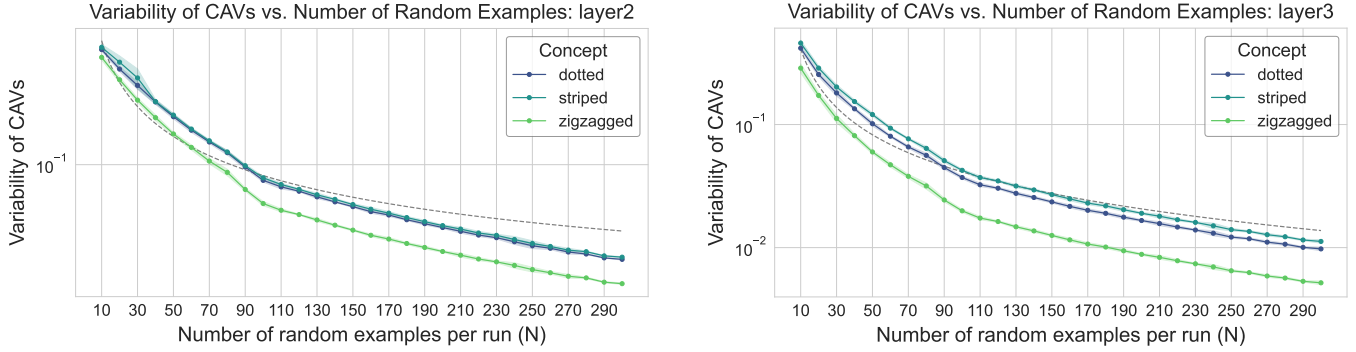


Figure 10: Mean variability of CAVs in dependence of the number of random examples per run N for **ResNet50 model**. The CAVs were generated using **difference-of-means**. Error bars indicate ± 1 SD; the y -axis is log-scaled. Variance is estimated by the sum of per-feature variances across five independent runs. We fitted a curve of the form $f(N) = a/N + b$ to it. For layer2 the parameters were $a = 7.24, b = 0.0106$, for layer3 they were $a = 4.13, b = 3.18 \times 10^{-8}$.

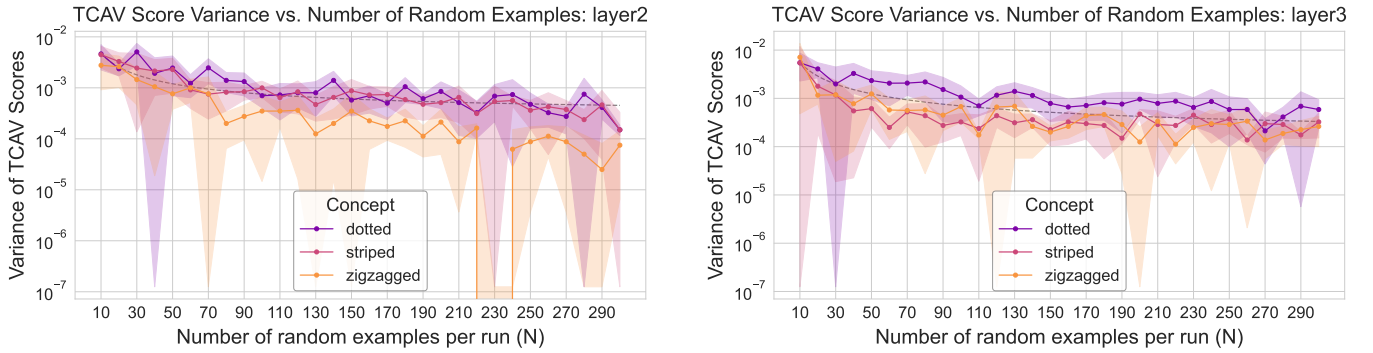


Figure 11: Variance of TCAV scores at 'layer2' and 'layer3' of the **ReseNet50 model** vs. the number N of random examples used. The underlying CAVs were generated using **difference-of-means**. Error bars denote ± 1 standard deviation. We fitted a curve of the form $f(N) = a/N + b$ to it. For layer2 the parameters were $a = 0.0429, b = 3.29 \times 10^{-4}$, for layer3 they were $a = 0.0548, b = 1.5 \times 10^{-4}$.

A.2 TCAV for Tabular

Because this tabular task is straightforward, we train several simple models from scratch. Using the Adult dataset(Becker and Kohavi 1996), we define two concepts from the gender field—male and female. In this setting, the results align best with our theory.

Empirical Findings with Binary Cross-Entropy Loss First, we analyze the results for tabular data, beginning with the binary cross-entropy loss from the logistic regression classifier.

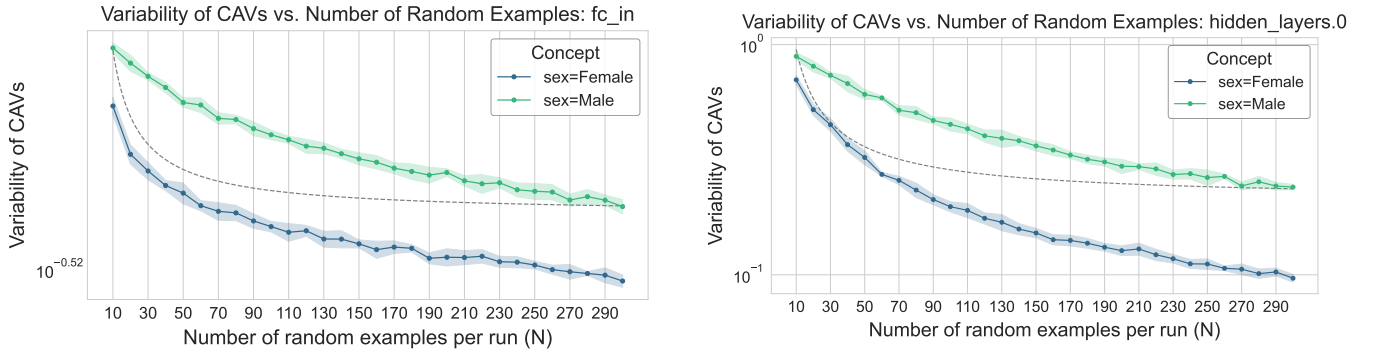


Figure 12: Mean variability of CAVs for the demographic concepts “male” and “female” as a function of the number of random examples per run (N) on the **UCI Adult dataset**. Results are shown for two different hidden layers. The linear classifiers for CAV generation were trained using **binary cross-entropy loss**. Error bars indicate ± 1 SD; the y -axis is log-scaled. Variance is estimated by the sum of per-feature variances across ten independent runs. We fitted a curve of the form $f(N) = a/N + b$ to it. For `fc_in` the parameters were $a = 4.65, b = 0.391$, for `hidden_layers_0` they were $a = 7.42, b = 0.212$.

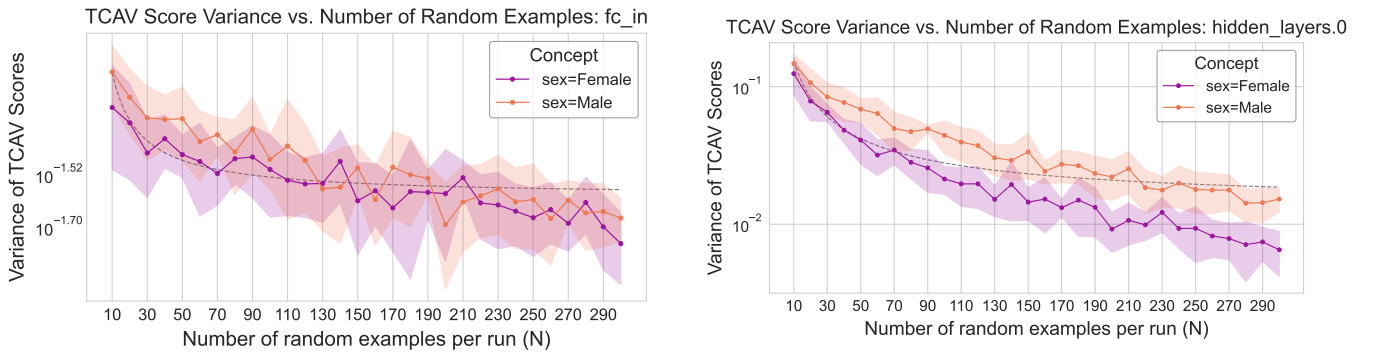


Figure 13: Variance of TCAV scores vs. the number of examples per concept set (N) for the concepts “male” and “female” on the **UCI Adult dataset**. The underlying CAVs were trained using **binary cross-entropy loss**. Error bars denote ± 1 standard deviation. We fitted a curve of the form $f(N) = a/N + b$ to it. For `fc_in` the parameters were $a = 0.407, b = 0.0254$, for `hidden_layers_0` they were $a = 1.4, b = 0.0139$.

Empirical Findings with Hinge Loss Following this, we examine the findings with hinge loss.

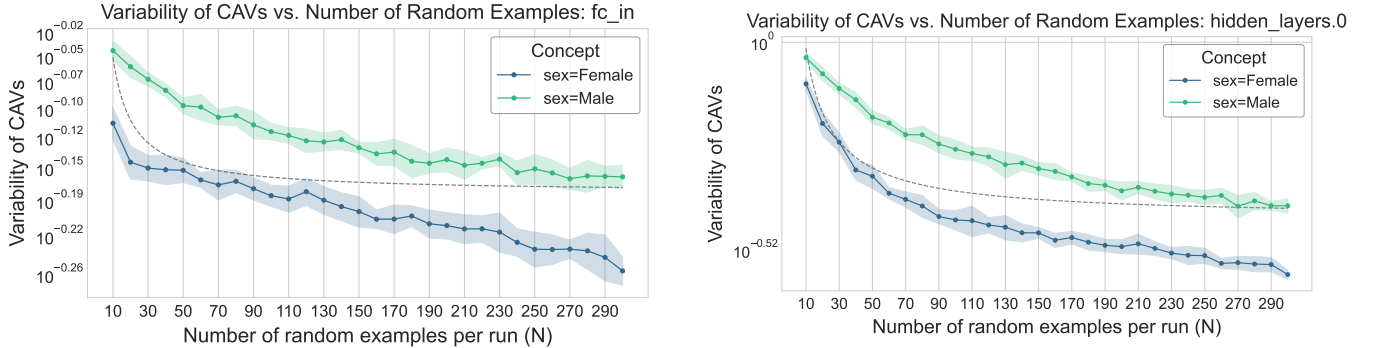


Figure 14: Mean variability of CAVs as a function of the number of random examples per run (N) on the **UCI Adult dataset**. Results are shown for two different hidden layers. The linear classifiers for CAV generation were trained using **hinge loss**. Variance is estimated by the sum of per-feature variances across ten independent runs. We fitted a curve of the form $f(N) = a/N + b$ to it. For `fc_in` the parameters were $a = 2.36, b = 0.662$, for `hidden_layers_0` they were $a = 6.04, b = 0.362$.

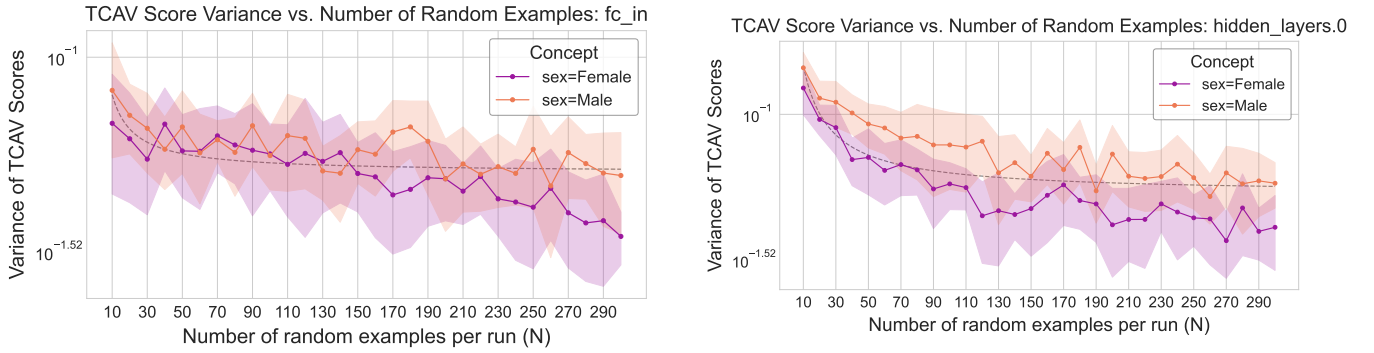


Figure 15: Variance of TCAV scores vs. the number of examples per concept set (N) for the concepts “male” and “female” on the **UCI Adult dataset**. The underlying CAVs were trained using **hinge loss**. Error bars denote ± 1 standard deviation. We fitted a curve of the form $f(N) = a/N + b$ to it. For `fc_in` the parameters were $a = 0.302, b = 0.049$, for `hidden_layers_0` they were $a = 0.976, b = 0.0518$.

Empirical Findings with Difference of Means When CAVs are computed via the *Difference of Means*-method, the variance decline best resembles an $\mathcal{O}(1/N)$ rate, compared to the other two methods we evaluated.

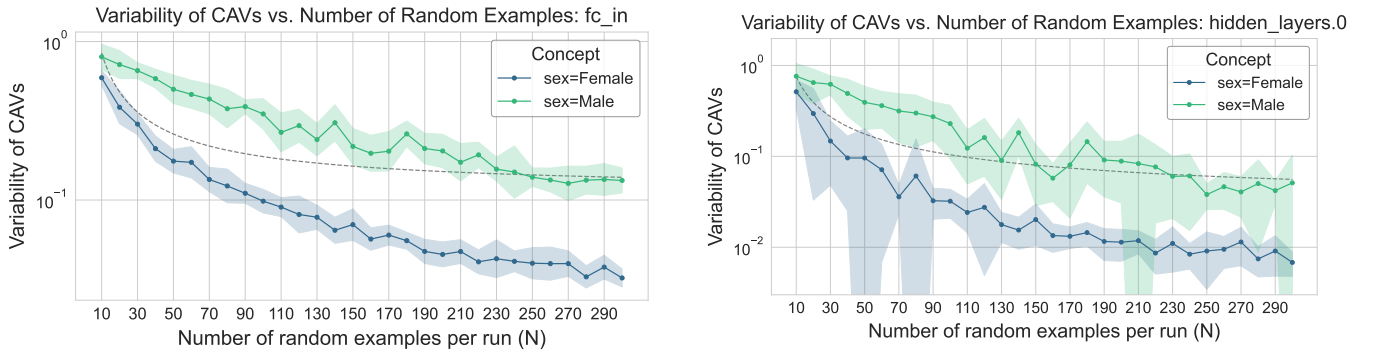


Figure 16: The linear classifiers for CAV generation were trained using **difference-of-means**. Error bars indicate ± 1 SD; the y -axis is log-scaled. Variance is estimated by the sum of per-feature variances across ten independent runs. We fitted a curve of the form $f(N) = a/N + b$ to it. For `fc_in` the parameters were $a = 7.31, b = 0.115$, for `hidden_layers_0` they were $a = 7.24, b = 0.0317$. Moreover, for `hidden_layers_0` we clipped below 3×10^{-3} to avoid visual distortion from extreme lows.

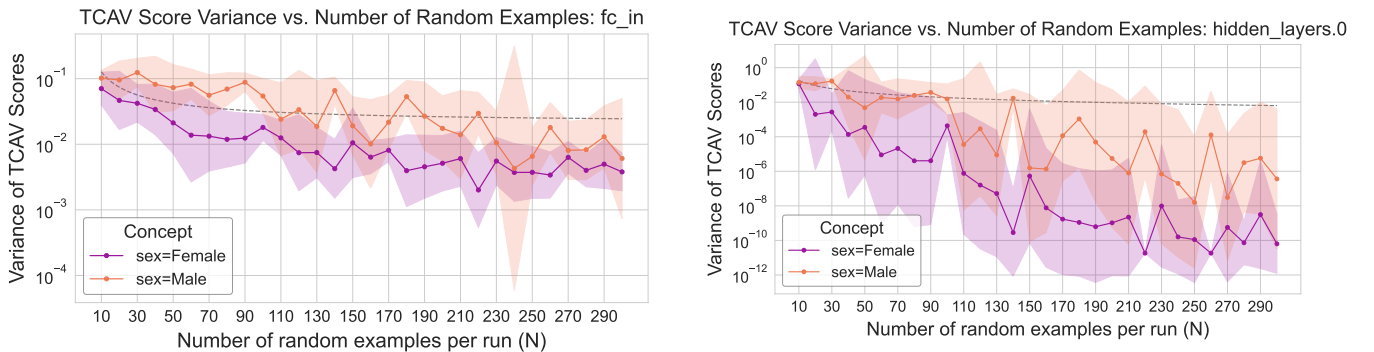


Figure 17: Mean geometrical variance of TCAV scores vs. the number of examples per concept set (N) for the concepts “male” and “female” on the **UCI Adult dataset**. The underlying CAVs were generated using **difference-of-means**. Error bars denote ± 1 geometrical standard deviation. We fitted a curve of the form $f(N) = a/N + b$ to it. For `fc_in` the parameters were $a = 1.06, b = 0.0209$, for `hidden_layers_0` they were $a = 1.81, b = 3.05 \times 10^{-4}$.

A.3 TCAV for Text

Empirical Findings with Binary Cross-Entropy Loss For the text data (**IMDB**), we first report the results from the logistic regression classifier using binary cross-entropy loss.

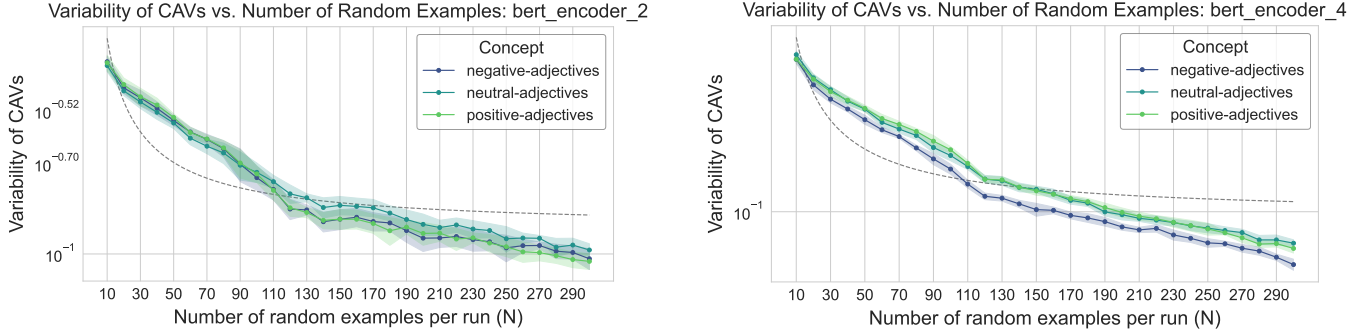


Figure 18: Mean variability of CAVs as a function of the number of random examples per run (N), shown for concepts at two different layers (bert_encoder_2 on the left, bert_encoder_4 on the right). Error bars indicate ± 1 SD; the y -axis is log-scaled. Variance is estimated by the sum of per-feature variances across ten runs. We fitted a curve of the form $f(N) = a/N + b$ to it. For bert_encoder_2 the parameters were $a = 4.02, b = 0.121$, for bert_encoder_4 they were $a = 4.27, b = 0.0958$.

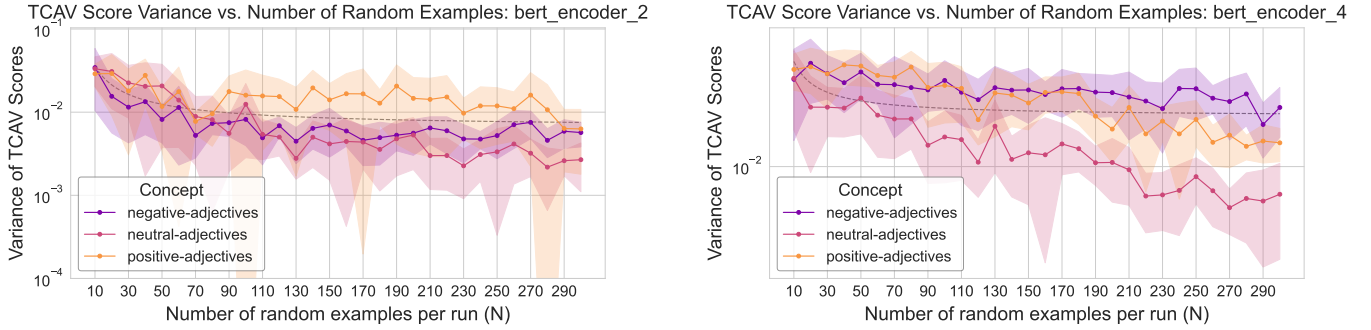


Figure 19: Variance of TCAV scores at layers bert_encoder_2 and bert_encoder_4 vs. the number of examples per concept set (N) for “positive”, “negative”, and “neutral”-adjective concepts on the IMDB dataset; error bars denote ± 1 standard deviation. We fitted a curve of the form $f(N) = a/N + b$ to it. For bert_encoder_2 the parameters were $a = 0.295, b = 0.00654$, for bert_encoder_4 they were $a = 0.329, b = 0.0226$. For bert_encoder_2 we cut the *log*- y -axis at $\geq 10^{-4}$ for readability to omit tiny standard deviation values.

Empirical Findings with Hinge Loss We now present the results for the `SGDLinearModel`, which uses hinge loss.

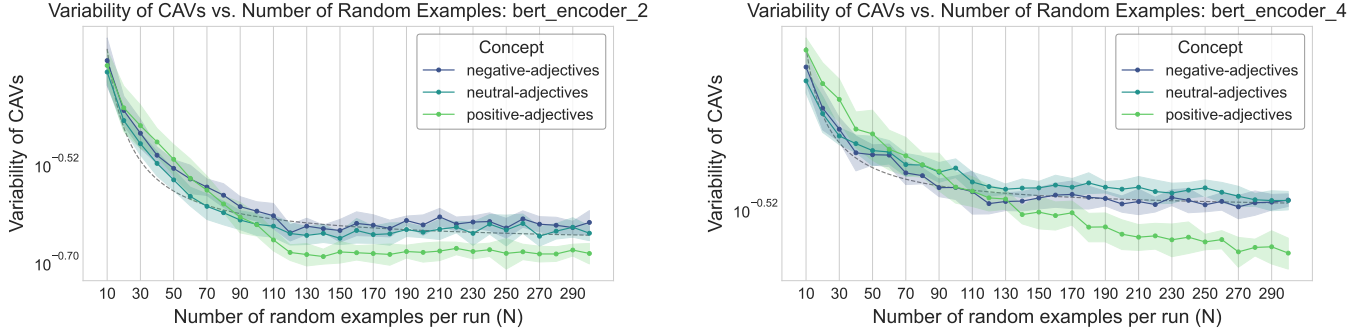


Figure 20: Mean variability of CAVs as a function of the number of random examples per run (N), shown for concepts at two different layers. Error bars indicate ± 1 SD; the y -axis is log-scaled. Variance is estimated by the sum of per-feature variances across ten runs. We fitted a curve of the form $f(N) = a/N + b$ to it. For `bert_encoder_2` the parameters were $a = 2.69, b = 0.215$, for `bert_encoder_4` they were $a = 3.02, b = 0.298$.

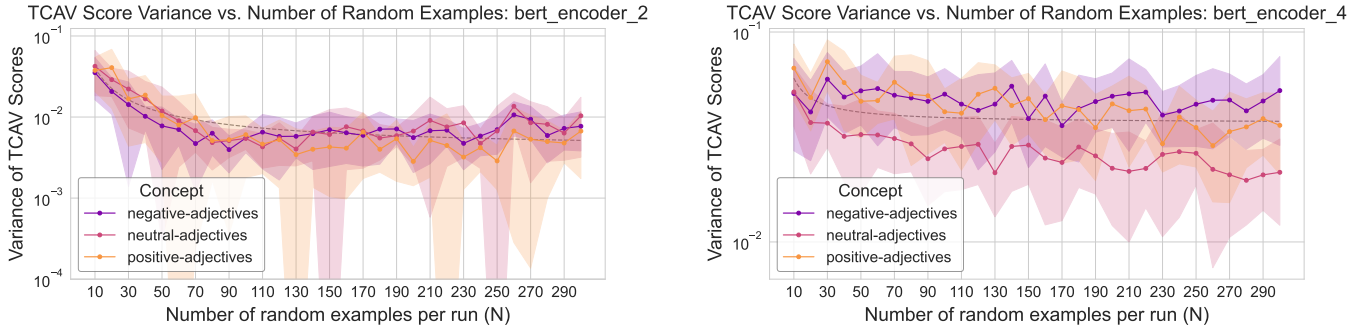


Figure 21: Variance of TCAV scores at layers `bert_encoder_2` and `bert_encoder_4` vs. the number of examples per concept set (N) for “positive”-, “negative”-, and “neutral”-adjective concepts on the IMDB dataset; error bars denote ± 1 standard deviation. We fitted a curve of the form $f(N) = a/N + b$ to it. For `bert_encoder_2` the parameters were $a = 0.372, b = 0.00391$ and cut the log scale at $\geq 10^{-4}$ so near-zero bands do not dominate. For `bert_encoder_4` the fitted parameters were $a = 0.235$ and $b = 0.0368$.

Empirical Findings with Difference of Means Again, we found that CAVs computed via the *Difference of Means*-method most closely follow a variance decline of $\mathcal{O}(1/N)$.

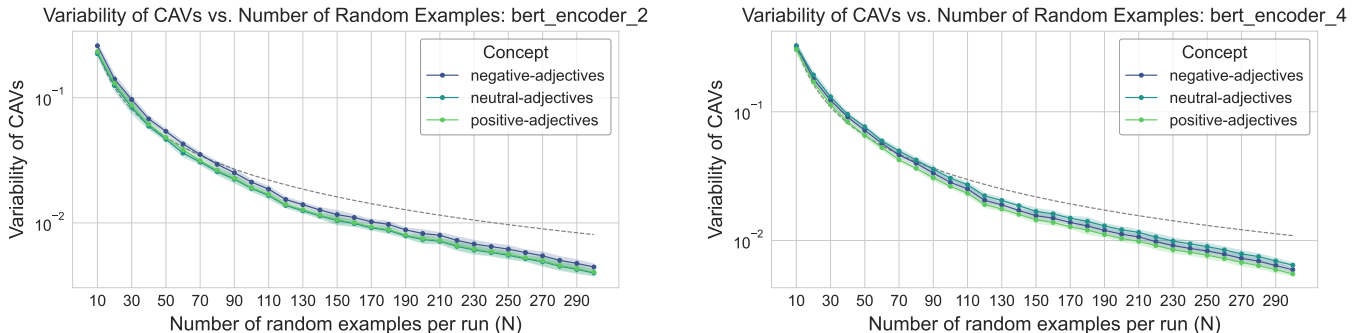


Figure 22: Mean variability of CAVs for the concepts “positive”, “negative” and “neutral” adjectives as a function of the number of random examples per run (N). Results are shown for two different hidden layers. The CAV are generated using **difference-of-means**. Error bars indicate ± 1 SD; the y -axis is log-scaled. Variance is estimated by the sum of per-feature variances across ten independent runs. We fitted a curve of the form $f(N) = a/N + b$ to it. For `bert_encoder_2` the parameters were $a = 2.42, b = 1.19 \times 10^{-7}$, for `bert_encoder_4` they were $a = 3.27, b = 3.24 \times 10^{-10}$.

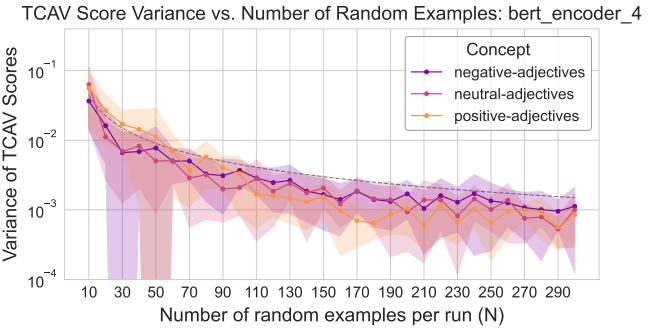
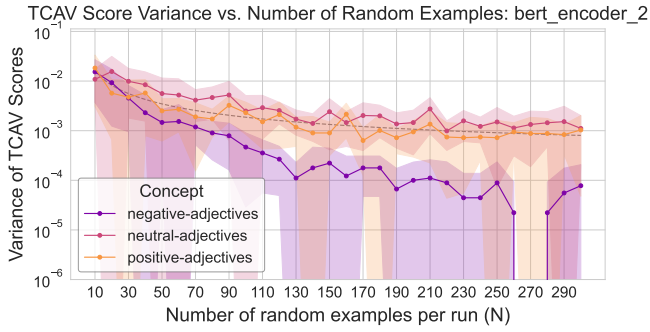


Figure 23: Variance of TCAV scores vs. the number of examples per concept set (N) for the concepts “positive”, “negative” and “neutral” adjectives. The underlying CAVs were generated using **difference-of-means**. Error bars denote ± 1 standard deviation. We fitted a curve of the form $f(N) = a/N + b$ to it. For `bert_encoder_2` the parameters were $a = 0.16, b = 2.7 \times 10^{-4}$, for `bert_encoder_4` they were $a = 0.449, b = 1.59 \times 10^{-8}$. We clipped below 10^{-6} respectively 10^{-4} to avoid visual distortion from extreme lows.

B Appendix B: Proofs of the Main Results

B.1 Asymptotic Normality with Binary Cross-Entropy Loss

In this section we present the proofs of the main results.

Setting and Notation. Recall that, for any $N > 0$, we set $\alpha_N \in \mathbb{R}$ and β_N the unique minimizers of the regularized loss (Eq. (4)). We also set $A_N := N e^{\alpha_N}$. Remember the following assumptions.

Assumption 1 (Surrounded Mean). *The distribution F_0 on \mathbb{R}^d has the point \bar{x} “surrounded,” that is*

$$\int_{(z-\bar{x})^\top \omega > \varepsilon} dF_0(z) > \delta \quad (5)$$

holds for some $\varepsilon > 0$, some $\delta > 0$ and all $\omega \in \Omega$ where $\Omega = \{\omega \in \mathbb{R}^d | \omega^\top \omega = 1\}$ is the unit sphere in \mathbb{R}^d and \bar{x} is the mean of the concept embeddings $\{x_i\}_{i=1}^n$.

Given this assumption, we can derive, analogous to Owen (2007), two consequences.

Corollary 2. *For describing this condition, we let $\Omega = \{\omega \in \mathbb{R}^d | \omega^\top \omega = 1\}$ be the unit sphere in \mathbb{R}^d . There is $\eta > 0$ such that*

$$\inf_{\omega \in \Omega} \int_{(z-\bar{x})^\top \omega \geq 0} dF_0(z) \geq \eta > 0 \quad \forall \omega \in \Omega. \quad (10)$$

Corollary 3. *Again let $\Omega = \{\omega \in \mathbb{R}^d | \omega^\top \omega = 1\}$ be the unit sphere in \mathbb{R}^d . Then there is $\gamma > 0$ such that*

$$\inf_{\omega \in \Omega} \int [(z - \bar{x})^\top \omega]_+ dF_0(z) \geq \gamma > 0. \quad (11)$$

Example visualization of Assumption 1 for the tabular setting is given in Figure 24. We provide the code to check this assumption in our notebooks.

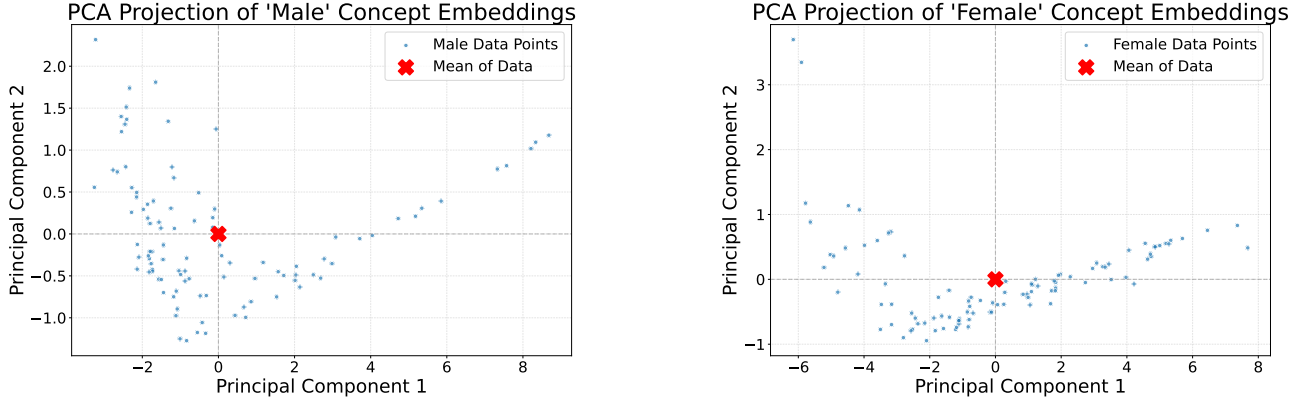


Figure 24: Geometric visualization of the surround assumption (Assumption 1) on the latent space. The 32-dimensional embeddings of the “Male” and “Female” concept are projected onto their first two principal components. The resulting scatter plot shows that the data points are not confined to a single half-space relative to their center, as they are distributed on all sides of the sample mean (red ‘X’).

The second assumption concerns the limit Hessian.

Assumption 2 (Limit Hessian). *Assume that the matrix H_0 , defined as the limit in probability of the normalized Hessian of the loss function,*

$$H_0 := \lim_{N \rightarrow \infty} \left(-\frac{1}{N} \nabla_\beta^2 \mathcal{L}^{(\lambda)}(\alpha_N, \beta_N) \right)$$

exists and is invertible.

This ensures that the limiting objective function is strictly convex at the solution, which is a standard requirement for proving asymptotic normality.

Furthermore, we must assume the convergence of our parameters so that an asymptotic consideration even takes on meaning. Unlike β , the intercept α is not consistent. However, we can adapt a weaker statement from Owen (2007) to our case.

Lemma 1 (Bounding for α_N (Lemma 6 in (Owen 2007))). Assume that Assumption 2 holds. For any $N \geq 2n/\eta$, we have $e^{\alpha_N} \leq 2 \frac{n}{N\eta}$.

Proof. Fix any $\beta_N \in \mathbb{R}^d$. Then

$$\nabla_{\alpha} \mathcal{L}_N^{(\lambda)} = n - \sum_{i=1}^n \frac{A_N N^{-1} e^{(x_i - \bar{x})^\top \beta_N}}{1 + A_N N^{-1} e^{(x_i - \bar{x})^\top \beta_N}} - N \int \frac{A_N N^{-1} e^{(z - \bar{x})^\top \beta_N}}{1 + A_N N^{-1} e^{(z - \bar{x})^\top \beta_N}} dF_0(z).$$

By the same bounding steps as in the un-penalized case (Owen 2007),

$$\nabla_{\alpha_N} \mathcal{L}_N^{(\lambda)} \leq n - \frac{A_N \eta}{1 + A_N/N}.$$

If $N \geq 2n/\eta$ but $A_N > 2n/\eta$, then

$$\frac{A_N \eta}{1 + A_N/N} > \frac{A_N \eta}{1 + (A_N \eta)/(2n)} > n,$$

so $\nabla_{\alpha_N} \mathcal{L}_N^{(\lambda)} < 0$. Concavity in α_N then forces

$$\alpha_N < \log(2n/\eta) - \log N \implies e^{\alpha_N} \leq \frac{2n}{N\eta}.$$

Since this holds for every β_N , the result follows. \square

Assumption 3 (Intercept Scaling Limit). The limit $A_0 = \lim_{N \rightarrow \infty} N e^{\alpha_N}$ exists.

This holds in practice as A_0 stabilizes with increasing N . For β , unlike α , we can assume that β is consistent.

Assumption 4 (Consistency of β). The log-likelihood function from (3), denoted by $\mathcal{L}_N(a, \beta)$, converges to a non-random, limiting function $\mathcal{L}_0(a, \beta)$ as $N \rightarrow \infty$. This limiting function is assumed to have an unique slope parameter, β_0 . Furthermore, the finite-sample maximizer, β_N converges to the true parameter β_0 , i.e., $\beta_N \xrightarrow{P} \beta_0$.

Given that β_N converges to the true unique slope parameter β_0 we can bound it asymptotically.

Lemma 2 (Bounding β_N (Lemma 7 in (Owen 2007))). Assume that Assumption 1 holds. Then

$$\limsup_{N \rightarrow \infty} \|\beta_N\| < \infty.$$

Proof. Let the regularized log-likelihood be $\mathcal{L}^{(\lambda)}(\alpha, \beta) = \mathcal{L}(\alpha, \beta) - \frac{\lambda}{2} \|\beta\|^2$. We analyze the behavior of the objective function by comparing its value at an arbitrary β to its value at $\beta = 0$

$$\begin{aligned} \mathcal{L}^{(\lambda)}(\alpha, 0) - \mathcal{L}^{(\lambda)}(\alpha, \beta) &= \left(\mathcal{L}(\alpha, 0) - \frac{\lambda}{2} \|0\|^2 \right) - \left(\mathcal{L}(\alpha, \beta) - \frac{\lambda}{2} \|\beta\|^2 \right) \\ &= \mathcal{L}(\alpha, 0) - \mathcal{L}(\alpha, \beta) + \frac{\lambda}{2} \|\beta\|^2. \end{aligned}$$

For the unregularized part, $\mathcal{L}(\alpha, 0) - \mathcal{L}(\alpha, \beta)$, we have:

$$\begin{aligned} \mathcal{L}(\alpha, 0) - \mathcal{L}(\alpha, \beta) &= -(n + N) \log(1 + e^\alpha) + \sum_{i=1}^n \log \left(1 + e^{\alpha + (x_i - \bar{x})^\top \beta} \right) \\ &\quad + N \int \log \left(1 + e^{\alpha + (x - \bar{x})^\top \beta} \right) dF_0(x). \end{aligned}$$

Since $\log(1 + e^y) > 0$ for any real y , both the summation and the integral terms are positive. We can therefore establish a simple lower bound

$$\mathcal{L}(\alpha, 0) - \mathcal{L}(\alpha, \beta) > -(n + N) \log(1 + e^\alpha).$$

Using the inequality $\log(1 + x) < x$ for $x > 0$, it follows that $\log(1 + e^\alpha) < e^\alpha$. Thus,

$$\mathcal{L}(\alpha, 0) - \mathcal{L}(\alpha, \beta) > -(n + N)e^\alpha.$$

Substituting this into the expression for the regularized difference, we obtain

$$\mathcal{L}^{(\lambda)}(\alpha, 0) - \mathcal{L}^{(\lambda)}(\alpha, \beta) > \frac{\lambda}{2} \|\beta\|^2 - (n + N)e^\alpha.$$

The objective function $\mathcal{L}^{(\lambda)}(\alpha, \beta)$ must be less than $\mathcal{L}^{(\lambda)}(\alpha, 0)$ whenever the right-hand side of this inequality is positive. This condition holds if

$$\frac{\lambda}{2} \|\beta\|^2 > (n + N)e^\alpha.$$

As in the original problem, we let $e^\alpha = A/N$. The condition becomes

$$\|\beta\|^2 > \frac{2(n + N)e^\alpha}{\lambda} = \frac{2(n + N)A/N}{\lambda} = \frac{2A}{\lambda} \left(1 + \frac{n}{N}\right).$$

Since the maximizer β_N cannot have an objective function value lower than at $\beta = 0$, its norm cannot satisfy the strict inequality above. Therefore, β_N must be bounded as follows

$$\|\beta\|_N^2 \leq \frac{2A}{\lambda} \left(1 + \frac{n}{N}\right).$$

We still rely on Lemma 1 to ensure that $A = Ne^\alpha$ remains bounded as $N \rightarrow \infty$. Given that, and since $n/N \rightarrow 0$ as $N \rightarrow \infty$, we can take the limit superior of the bound

$$\limsup_{N \rightarrow \infty} \|\beta_N\|^2 \leq \limsup_{N \rightarrow \infty} \frac{2A}{\lambda} \left(1 + \frac{n}{N}\right) = \frac{2 \sup(A)}{\lambda} < +\infty.$$

This proves that the norm of the regularized coefficient vector remains bounded as $N \rightarrow \infty$. It is important to note that this proof does not use Assumption 1. The L^2 regularization term itself ensures that the objective function is penalized for large values of β , making the assumption unnecessary for this result. \square

Lemma 3 (Asymptotic Consistency of a Penalized Mean (Theorem 8 in (Owen 2007))). *Assume that Assumptions 3 and 2 hold. Then*

$$\lim_{N \rightarrow +\infty} \int (z - \bar{x}) e^{z^\top \beta_N} dF_0(z) + \frac{\lambda e^{\bar{x}^\top \beta_N}}{N e^{\alpha_N}} \beta_N = 0, \quad (12)$$

that is,

$$\int (z - \bar{x}) e^{z^\top \beta_0} dF_0(z) = -\frac{\lambda e^{\bar{x}^\top \beta_0}}{A_0} \beta_0.$$

Remark 1. Eq. (12) is analogous to the relationship given in Theorem 8 of (Owen 2007). While the most apparent difference is the presence of the regularization term λ , this introduces a critical functional distinction. In (Owen 2007), the mapping defined by their relationship is proven to be injective. This injectivity, however, does not hold for our regularized mapping in Eq. (12), which complicates the analysis.

Proof. Using the necessary condition for a minimum, we set $\nabla_\beta \mathcal{L}_N^{(\lambda)}(\alpha_N, \beta_N) = 0$. This gives

$$-\sum_{j=1}^n (x_j - \bar{x}) \frac{e^{\alpha_N + \beta_N^\top (x_j - \bar{x})}}{1 + e^{\alpha_N + \beta_N^\top (x_j - \bar{x})}} - \sum_{i=1}^N (z_i - \bar{x}) \frac{e^{\alpha_N + \beta_N^\top (z_i - \bar{x})}}{1 + e^{\alpha_N + \beta_N^\top (z_i - \bar{x})}} - \lambda \beta_N = 0.$$

We analyze this equation in the limit as $N \rightarrow \infty$. By Lemma 2, $\|\beta_N\|$ is bounded, whereas by Lemma 1, $e^{\alpha_N} \rightarrow 0$. We deduce that

$$\lim_{N \rightarrow \infty} \left(-\sum_{j=1}^n (x_j - \bar{x}) \frac{e^{\alpha_N + \beta_N^\top (x_j - \bar{x})}}{1 + e^{\alpha_N + \beta_N^\top (x_j - \bar{x})}} \right) = 0.$$

We are left with the terms involving the random samples and the penalty

$$\lim_{N \rightarrow \infty} \left(-\sum_{i=1}^N (z_i - \bar{x}) \frac{e^{\alpha_N + \beta_N^\top (z_i - \bar{x})}}{1 + e^{\alpha_N + \beta_N^\top (z_i - \bar{x})}} - \lambda \beta_N \right) = 0.$$

Because the exponent $u_i = \alpha_N + \beta_N^\top (z_i - \bar{x}) \rightarrow -\infty$, we can apply the approximation $\frac{e^u}{1+e^u} \approx e^u$. This yields

$$\lim_{N \rightarrow \infty} \left(-\sum_{i=1}^N (z_i - \bar{x}) e^{\alpha_N + \beta_N^\top (z_i - \bar{x})} - \lambda \beta_N \right) = 0.$$

We factor the exponential term and rewrite the sum as N times an empirical average, which yields the result

$$\lim_{N \rightarrow \infty} \left(-N e^{\alpha_N} e^{-\beta_N^\top \bar{x}} \left[\frac{1}{N} \sum_{i=1}^N (z_i - \bar{x}) e^{\beta_N^\top z_i} \right] - \lambda \beta_N \right) = 0.$$

Applying Assumptions 4 and 3 to the equation gives

$$-A_0 e^{-\bar{x}^\top \beta_0} \int (z - \bar{x}) e^{z^\top \beta_0} dF_0(z) - \lambda \beta_0 = 0.$$

Finally, this yields

$$\int (z - \bar{x}) e^{z^\top \beta_0} dF_0(z) = -\frac{\lambda e^{\bar{x}^\top \beta_0}}{A_0} \beta_0.$$

□

Having recovered the limit equations for α and β , thereby extending the results of Owen (Owen 2007) to the L^2 -regularized case, we are now positioned to prove our main result on asymptotic normality.

Our proof strategy adapts the approach of Goldman and Zhang (Goldman and Zhang 2022). We will perform a higher-order Taylor expansion that leverages the key relationship derived in [Section/Eq. Y] to extract the necessary limiting dynamics. This approach establishes the following theorem, which generalizes Theorem 1 in (Goldman and Zhang 2022) to our more general regularized framework.

Theorem 1 (Asymptotic variability of CAVs). *Assume that Assumptions 1 and 2 hold, that the limit $A_0 = \lim_{N \rightarrow \infty} N e^{\alpha_N}$ exists and that $\beta_N \xrightarrow{p} \beta_0$, where \xrightarrow{p} denotes convergence in probability as $N \rightarrow \infty$. Then β_N is asymptotically normal. Namely,*

$$\sqrt{N}(\beta_N - \beta_0) \xrightarrow{D} \mathcal{N}(0, \Sigma), \quad (6)$$

where \xrightarrow{D} denotes convergence in distribution. A precise expression of Σ is given in Appendix B.1 (Eq. (18)).

Proof. We follow (Owen 2007; Goldman and Zhang 2022). The key difference is that we prove the asymptotic normality for the L^2 -regularized logistic regression estimator. We write

$$\begin{aligned} \mathcal{L}_N^{(\lambda)}(\alpha, \beta) &:= \sum_{i=1}^n \log \sigma(\alpha + \beta^\top (x_i - \bar{x})) \\ &+ \sum_{j=1}^N \log(1 - \sigma(\alpha + \beta^\top (z_j - \bar{x}))) - \frac{\lambda}{2} \|\beta\|^2 \end{aligned}$$

where \bar{x} is the mean of the concept samples $\{x_i\}$ with $y = 1$.

Since (α_N, β_N) maximize the log-likelihood, the gradient (score) vector evaluated at this point is zero. We focus on the gradient with respect to β :

$$\nabla_\beta \mathcal{L}_N^{(\lambda)}(\alpha_N, \beta_N) = 0.$$

By a Taylor expansion around β_0 ,

$$0 = \nabla_\beta \mathcal{L}_N^{(\lambda)}(\alpha_N, \beta_0) + \nabla_\beta^2 \mathcal{L}_N^{(\lambda)}(\alpha_N, \tilde{\beta}_N)(\beta_N - \beta_0) + o_p(1), \quad (13)$$

where the Hessian matrix $\nabla_\beta^2 \mathcal{L}^{(\lambda)}$ is evaluated at a point $\tilde{\beta}_N$ on the line segment between β_N and β_0 . Eq. (13) is simply Eq. (41) of (Goldman and Zhang 2022), the difference here is that $\nabla_\beta^2 \mathcal{L}^{(\lambda)}$ is modified to take regularization into account. Rearranging this expression gives the central equation for our analysis:

$$\sqrt{N}(\beta_N - \beta_0) = \left(-\frac{1}{N} \nabla_\beta^2 \mathcal{L}_N^{(\lambda)}(\alpha_N, \tilde{\beta}_N) \right)^{-1} \left(\frac{1}{\sqrt{N}} \nabla_\beta \mathcal{L}_N^{(\lambda)}(\alpha_N, \beta_0) \right) + o_p(1). \quad (14)$$

The proof proceeds by finding the asymptotic limits of the two terms on the right-hand side.

The Hessian matrix of our logistic regression loss (4) is given by:

$$\begin{aligned} \nabla_\beta^2 \mathcal{L}^{(\lambda)}(\alpha, \beta) &= - \sum_{k=1}^n \sigma_k(1 - \sigma_k)(x_k - \bar{x})(x_k - \bar{x})^\top \\ &- \sum_{k=1}^N \sigma_k(1 - \sigma_k)(z_k - \bar{x})(z_k - \bar{x})^\top - \lambda I. \end{aligned}$$

We analyze its behavior when normalized by $-1/N$. As $N \rightarrow \infty$, the contribution from the n fixed case terms and the penalty term $\lambda I/N$ both vanish. The dominant part arises from the N control terms. By the Law of Large Numbers and the consistency of the estimators, the normalized Hessian converges in probability to a constant, positive definite matrix H_0 :

$$-\frac{1}{N} \nabla_{\beta}^2 \mathcal{L}^{(\lambda)}(\alpha_N, \tilde{\beta}_N) \xrightarrow{p} H_0.$$

The scaled penalized score is:

$$\frac{1}{\sqrt{N}} \nabla_{\beta} \mathcal{L}_N^{(\lambda)}(\alpha_N, \beta_0) = \frac{1}{\sqrt{N}} \nabla_{\beta} \mathcal{L}_N(\alpha_N, \beta_0) - \frac{\lambda \beta_0}{\sqrt{N}}$$

with

$$\nabla_{\beta} \mathcal{L}_N(\alpha, \beta_0) = - \sum_{j=1}^n (x_j - \bar{x}) \frac{e^{\alpha + \beta_0^T (x_j - \bar{x})}}{1 + e^{\alpha + \beta_0^T (x_j - \bar{x})}} - \sum_{i=1}^N (z_i - \bar{x}) \frac{e^{\alpha + \beta_0^T (z_i - \bar{x})}}{1 + e^{\alpha + \beta_0^T (z_i - \bar{x})}}. \quad (15)$$

Crucially, the asymptotic parameter β_0 is the limit of the *penalized* optimization. By Lemma 3 we have the moment identity

$$\int (z - \bar{x}) e^{z^T \beta_0} dF_0(z) = -\frac{\lambda e^{\bar{x}^T \beta_0}}{A_0} \beta_0. \quad (16)$$

Under the rare-event scaling $Ne^{\alpha_N} \rightarrow A_0 \in (0, \infty)$ and using the expansion of the logistic link $\sigma(t) = e^t + O(e^{2t})$ as $t \rightarrow -\infty$, the unpenalized score at (α_N, β_0) admits the i.i.d.-sum representation

$$\frac{1}{\sqrt{N}} \nabla_{\beta} \mathcal{L}_N(\alpha_N, \beta_0) = \frac{1}{\sqrt{N}} \sum_{i=1}^N \tilde{\rho}(z_i; \beta_0) + r_N, \quad \tilde{\rho}(z; \beta_0) := -e^{\alpha_N - \beta_0^T \mu_0} (z - \mu_0) e^{z^T \beta_0}, \quad (17)$$

where $\mu_0 := \mathbb{E}_{F_0}[Z]$, the summands $\tilde{\rho}(z_i; \beta_0)$ are i.i.d., and the remainder satisfies $r_N = o_p(1)$. The remainder collects the $O(e^{2(\alpha_N + z^T \beta_0)})$ terms from the expansion of $\sigma(\alpha_N + z^T \beta_0)$; since $Ne^{\alpha_N} \rightarrow A_0$, we have $\sqrt{N} e^{2\alpha_N} = (Ne^{\alpha_N}) e^{\alpha_N} / \sqrt{N} \rightarrow 0$, which yields $r_N = o_p(1)$ under the moment condition $\mathbb{E}[\|Z\|^2 e^{2z^T \beta_0}] < \infty$. Because (17) uses μ_0 rather than the sample mean \bar{x} , it gives exact i.i.d. terms. Replacing μ_0 by \bar{x} only changes the right-hand side by $o_p(1)$ after the $1/\sqrt{N}$ scaling:

$$\frac{1}{\sqrt{N}} \sum_{i=1}^N \tilde{\rho}(z_i; \beta_0) = \frac{1}{\sqrt{N}} \sum_{i=1}^N \rho(z_i; \beta_0) + o_p(1), \quad \rho(z; \beta_0) := -e^{\alpha_N - \beta_0^T \bar{x}} (z - \bar{x}) e^{z^T \beta_0},$$

since $\sqrt{N}(\bar{x} - \mu_0) = O_p(1)$ while $e^{\alpha_N} = O(1/N)$. Finally, using (16),

$$\mathbb{E}[\tilde{\rho}(Z; \beta_0)] = -e^{\alpha_N - \beta_0^T \mu_0} \int (z - \mu_0) e^{z^T \beta_0} dF_0(z) = \frac{\lambda e^{\alpha_N}}{A_0} \beta_0,$$

so the mean contribution to $N^{-1/2} \sum_{i=1}^N \tilde{\rho}(z_i; \beta_0)$ is $\sqrt{N} \mathbb{E}[\tilde{\rho}(Z; \beta_0)] = O(\sqrt{N} e^{\alpha_N}) \rightarrow 0$ under $Ne^{\alpha_N} \rightarrow A_0$. This justifies the zero-centering in (17). This expectation is non-zero in the penalized case:

$$\begin{aligned} \mathbb{E}[\rho(z; \beta_0)] &= -e^{\alpha_N - \beta_0^T \bar{x}} \int (z - \bar{x}) e^{z^T \beta_0} dF_0(z) \\ &= -e^{\alpha_N - \beta_0^T \bar{x}} \left(-\frac{\lambda e^{\bar{x}^T \beta_0}}{A_0} \beta_0 \right) \\ &= \frac{e^{\alpha_N}}{A_0} \lambda \beta_0. \end{aligned}$$

We now rewrite the full penalized score by explicitly centring the sum:

$$\frac{1}{\sqrt{N}} \nabla_{\beta} \mathcal{L}_N^{(\lambda)}(\alpha_N, \beta_0) = \underbrace{\frac{1}{\sqrt{N}} \sum_{i=1}^N (\rho(z_i) - \mathbb{E}[\rho])}_{\text{Zero-mean part}} + \underbrace{\sqrt{N} \cdot \mathbb{E}[\rho]}_{\text{Mean part}} - \frac{\lambda \beta_0}{\sqrt{N}} + o_p(1).$$

Let us analyze the mean part. Since by definition $A_0 = \lim_{N \rightarrow \infty} Ne^{\alpha_N}$, we have:

$$\sqrt{N} \cdot \mathbb{E}[\rho] = \sqrt{N} \cdot \frac{e^{\alpha_N}}{A_0} \lambda \beta_0 = \frac{\lambda \beta_0}{\sqrt{N}} + o(1/\sqrt{N}).$$

Substituting this back, we get:

$$\frac{1}{\sqrt{N}} \nabla_{\beta} \mathcal{L}_N^{(\lambda)}(\alpha_N, \beta_0) = \frac{1}{\sqrt{N}} \sum_{i=1}^N (\rho(z_i) - \mathbb{E}[\rho]) + \frac{\lambda \beta_0}{\sqrt{N}} - \frac{\lambda \beta_0}{\sqrt{N}} + o_p(1).$$

The scaled penalized score is therefore asymptotically equivalent to a sum of i.i.d. random variables with a true zero mean. By the Central Limit Theorem, this sum converges in distribution to a Normal random variable.

$$\frac{1}{\sqrt{N}} \nabla_{\beta} \mathcal{L}_N^{(\lambda)}(\alpha_N, \beta_0) \xrightarrow{D} \mathcal{N}(0, \Sigma'),$$

where

$$\Sigma' = \text{Var}_{F_0}(\rho(z; \beta_0)).$$

As the penalty term vanishes, the scaled penalized score has the same limiting distribution as the unpenalized score.

Substituting these results back into Eq. (14) gives

$$\sqrt{N}(\beta_N - \beta_0) = \underbrace{\left(-\frac{1}{N} \nabla_{\beta}^2 \mathcal{L}^{(\lambda)} \right)^{-1}}_{\xrightarrow{P} H_0^{-1}} \underbrace{\left(\frac{1}{\sqrt{N}} \nabla_{\beta} \mathcal{L}_N^{(\lambda)} \right)}_{\xrightarrow{D} \mathcal{N}(0, \text{Var}_{F_0}(\rho(z; \beta_0)))} + o_p(1).$$

By Slutsky's Theorem (Slutzky 1937) and under Assumption 2, the product converges in distribution. This yields the final result:

$$\sqrt{N}(\beta_N - \beta_0) \xrightarrow{D} \mathcal{N}(0, \Sigma),$$

where the asymptotic covariance matrix is given by

$$\Sigma := H_0^{-1} \text{Var}_{F_0}(\rho(z; \beta_0)) (H_0^{-1})^{\top} \quad (18)$$

This completes the proof. \square

To extend this result to the real asymptotic convergence behaviour of our Concept Activation Vectors, we need the notation of *uniform integrability* (Vaart 2007).

Definition 2 (Uniform Integrability). A sequence of random variables $\{X_N\}_{N \geq 1}$ is uniformly integrable if

$$\lim_{K \rightarrow \infty} \sup_{N \geq 1} E[|X_N| \cdot \mathbf{1}_{\{|X_N| > K\}}] = 0.$$

Now we can prove the following corollary about the asymptotic behavior of the covariance trace.

Corollary 4 (Asymptotic Behavior of the Covariance Trace). Under the assumptions of Theorem 1 and uniform integrability, the asymptotic covariance matrix of the estimator β_N is proportional to $\frac{1}{N} \Sigma$. Consequently, the trace of the covariance matrix $\text{Var}(\beta_N)$ is of order $\mathcal{O}(N^{-1})$.

Proof. Theorem 1 states that:

$$\sqrt{N}(\beta_N - \beta_0) \xrightarrow{D} \mathcal{N}(0, \Sigma)$$

Uniform integrability also ensures the convergence of the relevant moments (Vaart 2007, Theorem 2.20). Therefore, the covariance matrix of the sequence of random variables converges to the covariance matrix of the limiting distribution. This allows us to write the exact limit:

$$\lim_{N \rightarrow \infty} \text{Cov}(\sqrt{N}(\beta_N - \beta_0)) = \Sigma \quad (19)$$

Using the properties of the covariance operator, where β_0 is a constant vector and N is a scalar, we have the identity:

$$\text{Cov}(\sqrt{N}(\beta_N - \beta_0)) = N \cdot \text{Cov}(\beta_N)$$

Substituting this identity into the limit expression from (19) yields:

$$\lim_{N \rightarrow \infty} (N \cdot \text{Cov}(\beta_N)) = \Sigma$$

This equation formally states that the asymptotic covariance matrix of the scaled estimator $\sqrt{N}\beta_N$ is Σ . For a finite but large N , this implies that $\text{Cov}(\beta_N)$ is well-approximated by $\frac{1}{N}\Sigma$. This justifies the corollary's statement that the covariance is proportional to $\frac{1}{N}\Sigma$.

The variance is defined as the trace of the covariance matrix: $\text{Var}(\beta_N) := \text{tr}(\text{Cov}(\beta_N))$. We apply the trace operator to the limit we derived in Part 1. Since the trace is a continuous linear map on the space of matrices, it commutes with the limit operator:

$$\begin{aligned}\text{tr}(\Sigma) &= \text{tr}\left(\lim_{N \rightarrow \infty} N \cdot \text{Cov}(\beta_N)\right) \\ &= \lim_{N \rightarrow \infty} \text{tr}(N \cdot \text{Cov}(\beta_N)) \\ &= \lim_{N \rightarrow \infty} (N \cdot \text{tr}(\text{Cov}(\beta_N))) \\ &= \lim_{N \rightarrow \infty} (N \cdot \text{Var}(\beta_N))\end{aligned}$$

So we have the precise limit:

$$\lim_{N \rightarrow \infty} (N \cdot \text{Var}(\beta_N)) = \text{tr}(\Sigma)$$

Since Σ is a constant matrix, its trace $\text{tr}(\Sigma)$ is a finite constant. Setting $a_N = \text{Var}(\beta_N)$ and $f(N) = N^{-1}$, our limit shows:

$$\lim_{N \rightarrow \infty} \frac{\text{Var}(\beta_N)}{N^{-1}} = \text{tr}(\Sigma)$$

This directly implies that $\text{Var}(\beta_N) = \mathcal{O}(N^{-1})$, which concludes the proof. \square

B.2 Asymptotic Normality with Hinge Loss

By default, the TCAV implementations in both TensorFlow and PyTorch use `sklearn's SGDClassifier` (Pedregosa et al. 2011), which operates by minimizing the hinge loss function. It achieves this by penalizing predictions that are not only incorrect but also those that are correct but fall within a specified “margin” around the decision boundary.

For a dataset of $N + n$ samples $\{(u_i, y_i)\}_{i=1}^{N+n}$ with true labels $y_i \in \{-1, 1\}$, the final loss $J_N^{(\lambda)}(\beta, \alpha)$ minimized is defined as the sum of the average hinge loss and an L^2 regularization term:

$$J_N^{(\lambda)}(\beta, \alpha) = \left(\frac{1}{N+n} \sum_{i=1}^{N+n} \max[0, 1 - y_i(\beta^\top u_i + \alpha)] \right) + \frac{\lambda}{2} \|\beta\|^2.$$

Here, λ represents the regularization strength hyperparameter, β is the weight vector, and α is the intercept term. Again we consider our known setting. The only difference is that we use a different labeling system.

The first class consists of n fixed points, $\{x_i\}_{i=1}^n \subset \mathbb{R}^d$, referred to as “concept” samples with label $y = 1$. The second class consists of N random points, $\{z_j\}_{j=1}^N \subset \mathbb{R}^d$, drawn independently and identically from a distribution F_0 with label $y = -1$.

For our main theorem of asymptotic normality to hold, we require the following assumptions:

1. The distribution F_0 of the controls must be continuous.

Specifically, the projection $\beta_0^\top Z$ must have a continuous probability density function, $f_{\beta_0^\top Z}(\cdot)$, in a neighbourhood of -1 .

2. The distribution F_0 must have finite second moments, i.e., $\mathbb{E}_{Z \sim F_0}[\|Z\|^2] < \infty$.

Given these assumptions we can now state the theorem.

Theorem 1 (Asymptotic Normality with Hinge Loss). *Let β_N be the minimizer of the objective function $J_N(\beta)$. Let β_0 be the unique minimizer of the limiting objective function*

$$\lim_{N \rightarrow \infty} J_N^{(\lambda)}(\beta, \alpha) = \mathbb{E}_{Z \sim F_0}[\max(0, 1 + \beta^\top Z + \alpha)] + \frac{\lambda}{2} \|\beta\|^2. \quad (20)$$

Under the assumptions listed above in Section B.2, as $N \rightarrow \infty$ with n fixed, the estimator is asymptotically normal:

$$\sqrt{N}(\beta_N - \beta_0) \xrightarrow{D} \mathcal{N}(0, M^{-1} \Sigma_Z M^{-1}), \quad (21)$$

where $M = \lambda I + \mathbb{E}[ZZ^\top | \beta_0^\top Z = -1] f_{\beta_0^\top Z}(-1)$, and $\Sigma_Z = \text{Var}(Z \cdot I(\beta_0^\top Z > -1))$.

Proof. As $N \rightarrow \infty$, the objective function $J_N(\beta)$ converges pointwise in probability to $\lim_{N \rightarrow \infty} J_N^{(\lambda)}(\beta)$. Under standard M-estimation arguments, the minimizer β_N of $J_N(\beta)$ converges in probability to the minimizer β_0 of $\lim_{N \rightarrow \infty} J_N^{(\lambda)}(\beta)$.

We first perform a Taylor expansion of the gradient of the objective function around β_0 , and set $\nabla J_N(\beta_N) = 0$:

$$0 = \nabla_\beta J_N(\beta_0) + \nabla_\beta^2 J_N(\beta_0)(\beta_N - \beta_0) + o_p(1). \quad (22)$$

Rearranging gives

$$\sqrt{N}(\beta_N - \beta_0) = -[\nabla_{\beta}^2 J_N(\beta_0)]^{-1} \sqrt{N} \nabla_{\beta} J_N(\beta_0) + o_p(1).$$

We analyze the two terms on the right. The optimality of β_0 for the limiting problem implies $\lim_{N \rightarrow \infty} \nabla_{\beta} J^{(\lambda)}(\beta) = 0$. This gives the condition $\mathbb{E}[Z \cdot I(\beta_0^T Z > -1)] + \lambda \beta_0 = 0$. Let now $\mu_0 = \mathbb{E}[Z \cdot I(\beta_0^T Z > -1)]$. The gradient of the finite-sample objective at β_0 is

$$\begin{aligned} \nabla_{\beta} J_N(\beta_0) &= \frac{N}{n+N} \left(\frac{1}{N} \sum_{j=1}^N z_j I(\beta_0^T z_j > -1) - \mu_0 \right) \\ &\quad - \frac{n}{n+N} \left(\frac{1}{n} \sum_{i=1}^n x_i I(\beta_0^T x_i < 1) + \mu_0 \right). \end{aligned}$$

When scaled by \sqrt{N} , the second term vanishes as $N \rightarrow \infty$. By the Central Limit Theorem and our assumption on $\mathbb{E}_{Z \sim F_0}[\|Z\|^2] < \infty$, the first term converges in distribution. Thus, the scaled score has a normal limit

$$\sqrt{N} \nabla_{\beta} J_N(\beta_0) \xrightarrow{D} \mathcal{N}(0, \Sigma_Z) \quad (23)$$

where $\Sigma_Z = \text{Var}(Z \cdot I(\beta_0^T Z > -1))$. The Hessian matrix of the finite-sample objective, $H_N(\beta) = \nabla_{\beta}^2 J_N(\beta)$, converges in probability to the Hessian of the limiting objective

$$H := \lim_{N \rightarrow \infty} \nabla_{\beta}^2 J_N(\beta_0) = \lambda I + \mathbb{E}[ZZ^T | \beta_0^T Z = -1] f_{\beta_0^T Z}(-1). \quad (24)$$

Slutsky's Theorem (Slutzky 1937) and the assumed probability density function, $f_{\beta_0^T Z}(\cdot)$ give us the asymptotic distribution of the estimator

$$\sqrt{N}(\beta_N - \beta_0) \xrightarrow{D} \mathcal{N}(0, H^{-1} \Sigma_Z H^{-1}).$$

This completes the proof. \square

B.3 Asymptotic Normality of Difference of Means

The Difference of Means (DoM) (Martin 2019) method identifies a concept's direction within a model's activation space by simply taking the vector difference between the average activation for concept examples and the average activation for random examples. As this method was also adapted for calculating CAVs (Santis et al. 2024), we analyze the stability of the direction vector $\beta_N = \bar{x} - \bar{z}$, where \bar{x} is the mean of the n fixed concept samples and \bar{z} is the mean of N random samples (from an independent distribution F_0 with covariance Σ_z).

Theorem 2 (Asymptotic Variance of the Difference of Means Vector). *Let $\{x_i\}_{i=1}^n$ be n fixed points, and let $\{z_j\}_{j=1}^N$ be N random samples drawn i.i.d. from an independent distribution F_0 with finite covariance Σ_z . Define the direction vector $\beta_N = \bar{x} - \bar{z}$ as the difference of the respective means.*

Then, the total variance of β_N , is given by:

$$\text{tr}(\text{Cov}(\beta_N)) = \frac{1}{N} \text{tr}(\Sigma_z) \quad (25)$$

Proof. The variance of β_N , measured by $\text{tr}(\text{Cov}(\beta_N))$, is derived as follows. Since the set $\{x_i\}_{i=1}^n$ is fixed, their mean \bar{x} is a deterministic constant vector, and thus $\text{Cov}(\bar{x}) = 0$. The variance of β_N is therefore determined exclusively by the random component \bar{z} .

$$\text{tr}(\text{Cov}(\beta_N)) = \text{tr}(\text{Cov}(\bar{x} - \bar{z})) \quad (26)$$

$$= \text{tr}(\text{Cov}(\bar{z})) \quad (\text{since } \bar{x} \text{ is a fixed constant}) \quad (27)$$

$$= \text{tr} \left(\text{Cov} \left(\frac{1}{N} \sum_{j=1}^N z_j \right) \right) \quad (28)$$

$$= \text{tr} \left(\frac{1}{N^2} \sum_{j=1}^N \text{Cov}(z_j) \right) \quad (\text{by i.i.d. assumption}) \quad (29)$$

$$= \text{tr} \left(\frac{1}{N^2} (N \cdot \Sigma_z) \right) \quad (30)$$

$$= \text{tr} \left(\frac{1}{N} \Sigma_z \right) \quad (31)$$

$$= \frac{1}{N} \text{tr}(\Sigma_z) \quad (32)$$

Since $\text{tr}(\Sigma_z)$ is a fixed constant, the variance of β_N declines at a rate of $\mathcal{O}(1/N)$ as the number of random samples N increases. \square

As the number of random samples $N \rightarrow \infty$ (while n remains fixed), the variance of β_N converges to zero at a rate of $\mathcal{O}(1/N)$. The *Difference of Means*-method thus exhibits the same convergence behaviour as the other two classifiers discussed.